ACME
Astrophysics Centre for Multimessenger studies in Europe

Funded by the European Union

Kilonovae: Theory and Modelling

Stefano Ascenzi (GSSI)

stefano.ascenzi@gssi.it

Image Credit: Mark Garlick

Introduction

The tutor

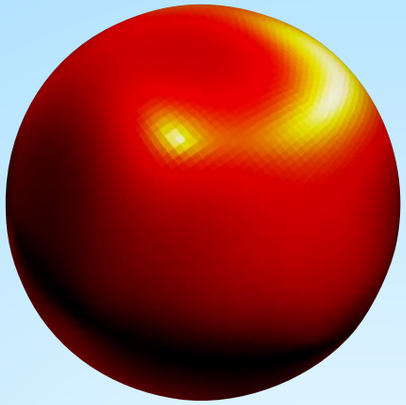

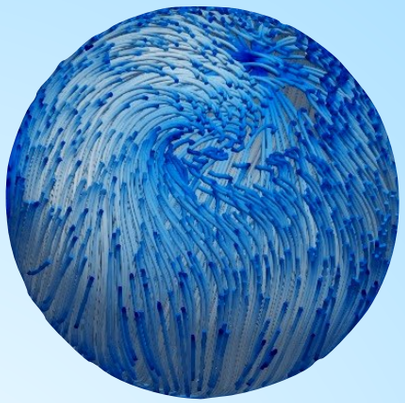

Magneto-thermal simulations of magnetars and modelling of their electromagnetic emission (MATINS 3D code)

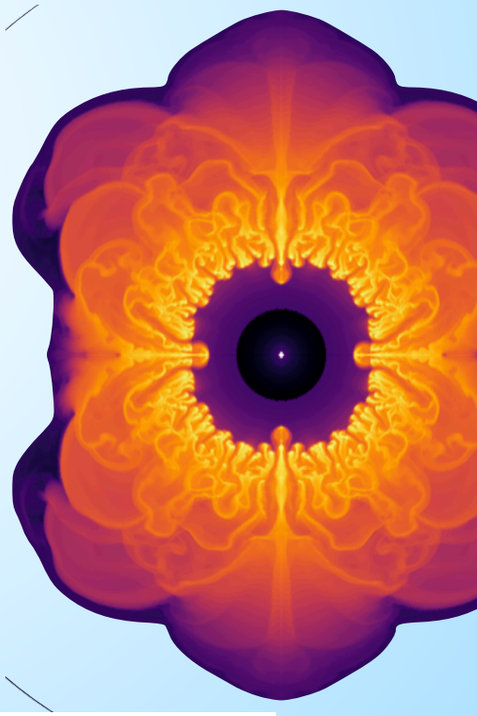

Modelling Electromagnetic Counterparts of Compact Binary Mergers (SGRB + Kilonovae + Spindown-powered transients) through semi-analytical and numerical methods

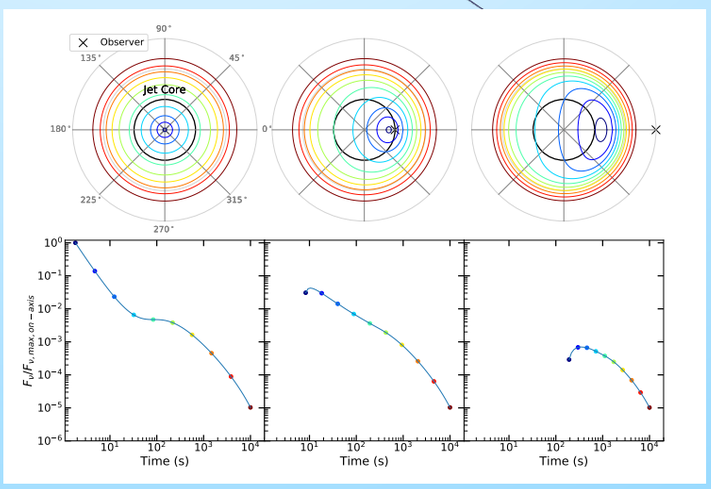

GRAN SASSO SCIENCE INSTITUTE

SCHOOL OF ADVANCED STUDIES

Scuola Universitaria Superiore

Outline of the tutorial

- Observational Introduction
- Kilonova in a nutshell
- A Kilonova Toy-model

- Microphysics of Kilonovae
- Multiple component Kilonovae

- How we model Kilonovae

GW170817

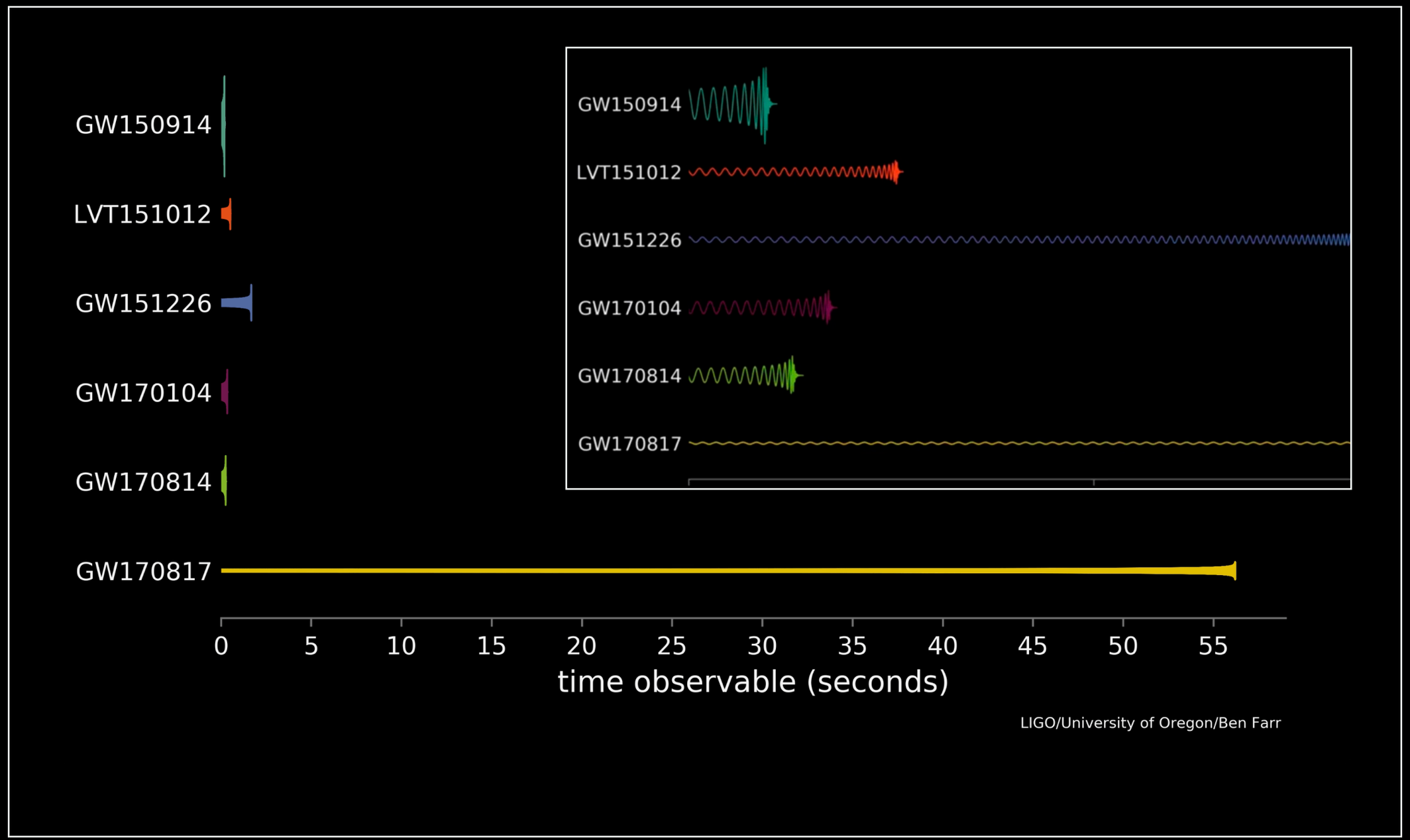
GW150914
LVT151012
GW151226
GW170104
GW170814
GW170817
0
5
10
15
20
25
30
35
40
45
50
55
time observable (seconds)
LIGO/University of Oregon/Ben Farr

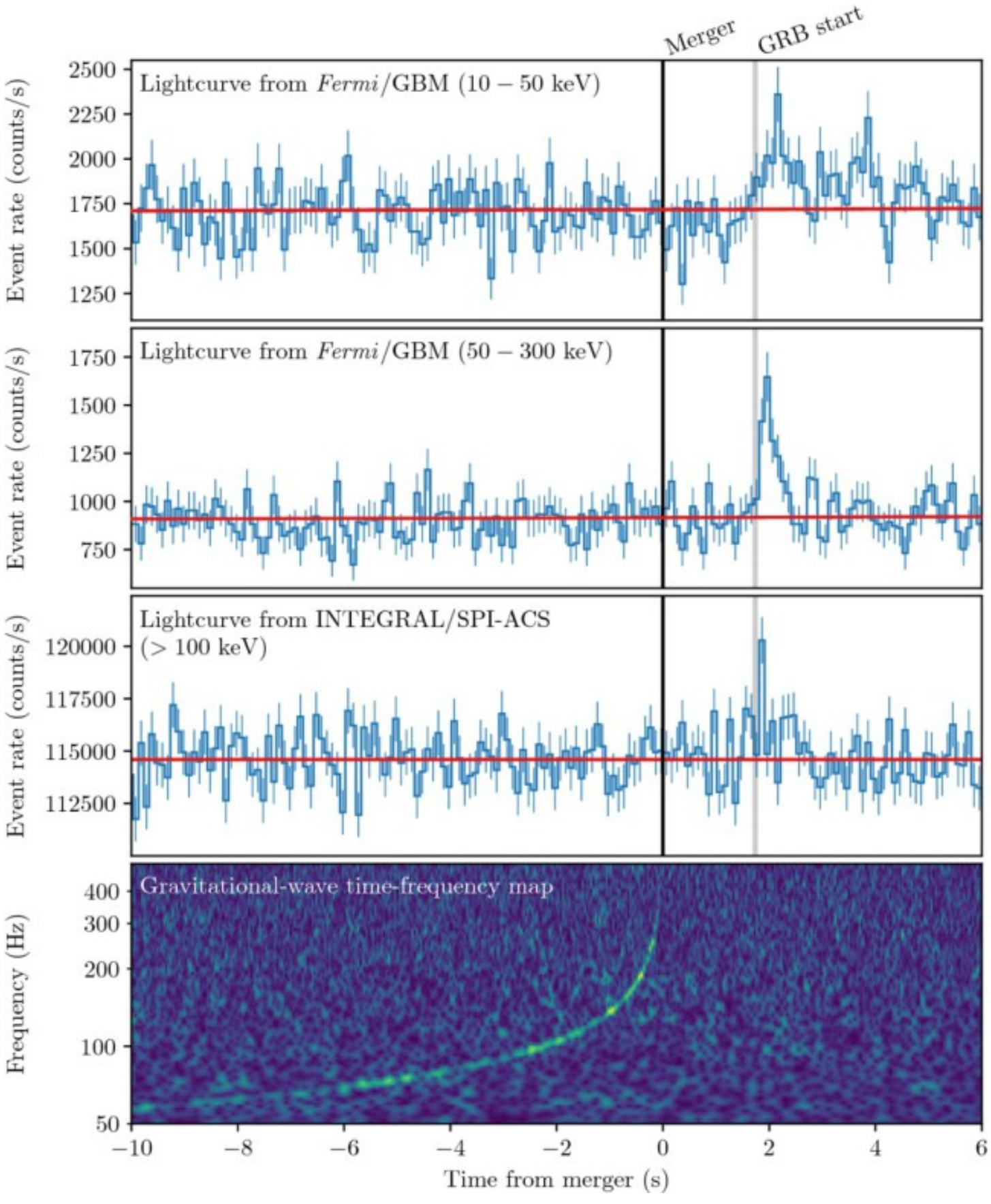

γ – rays

GW

(LVC, Fermi & Integral Collaborations, 2017)

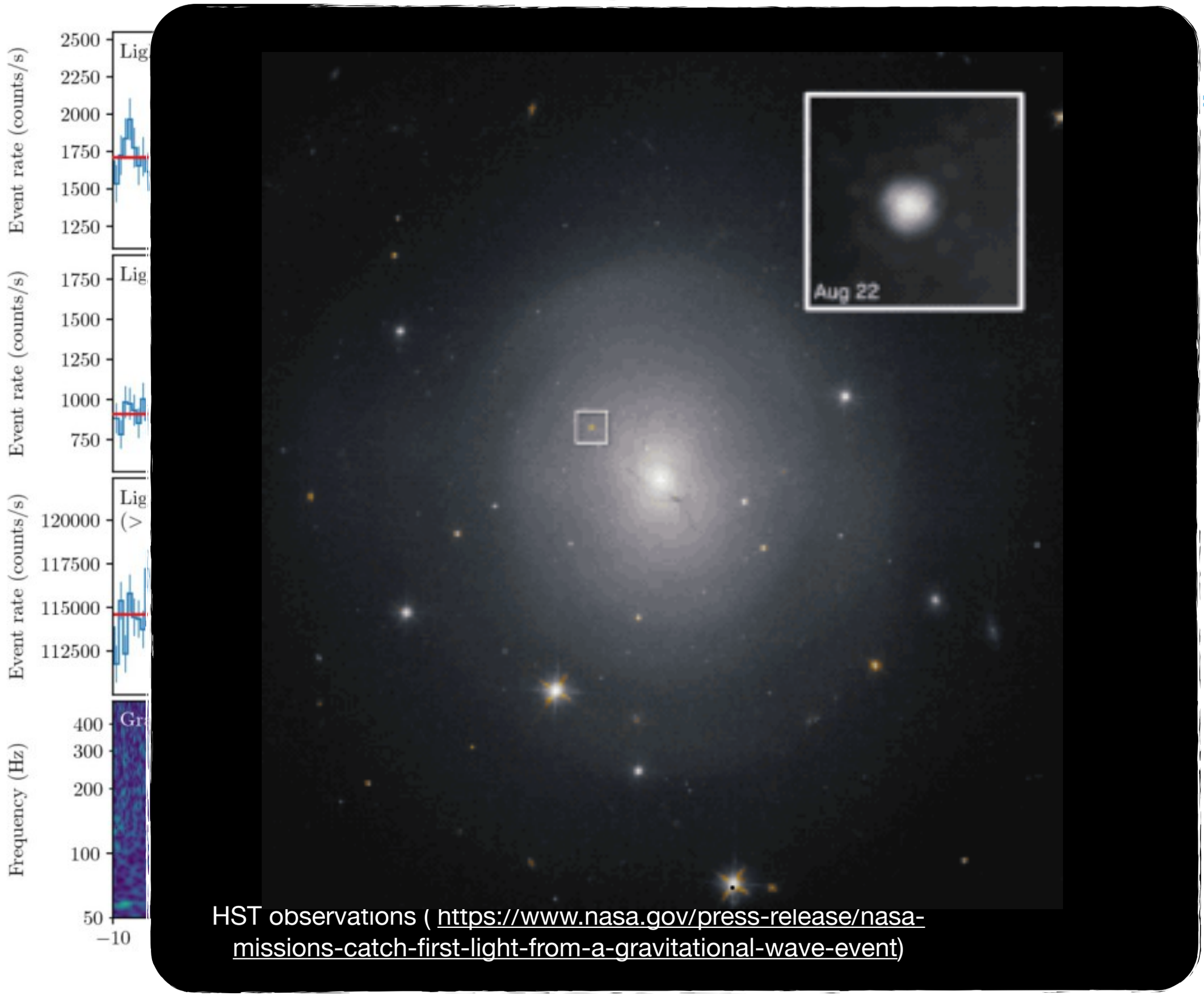

HST observations (https://www.nasa.gov/press-release/nasa-missions-catch-first-light-from-a-gravitational-wave-event)

(LVC, Fermi & Integral Collaborations, 2017)

Optical/NIR Spectra

ESO-VLT/X-Shooter

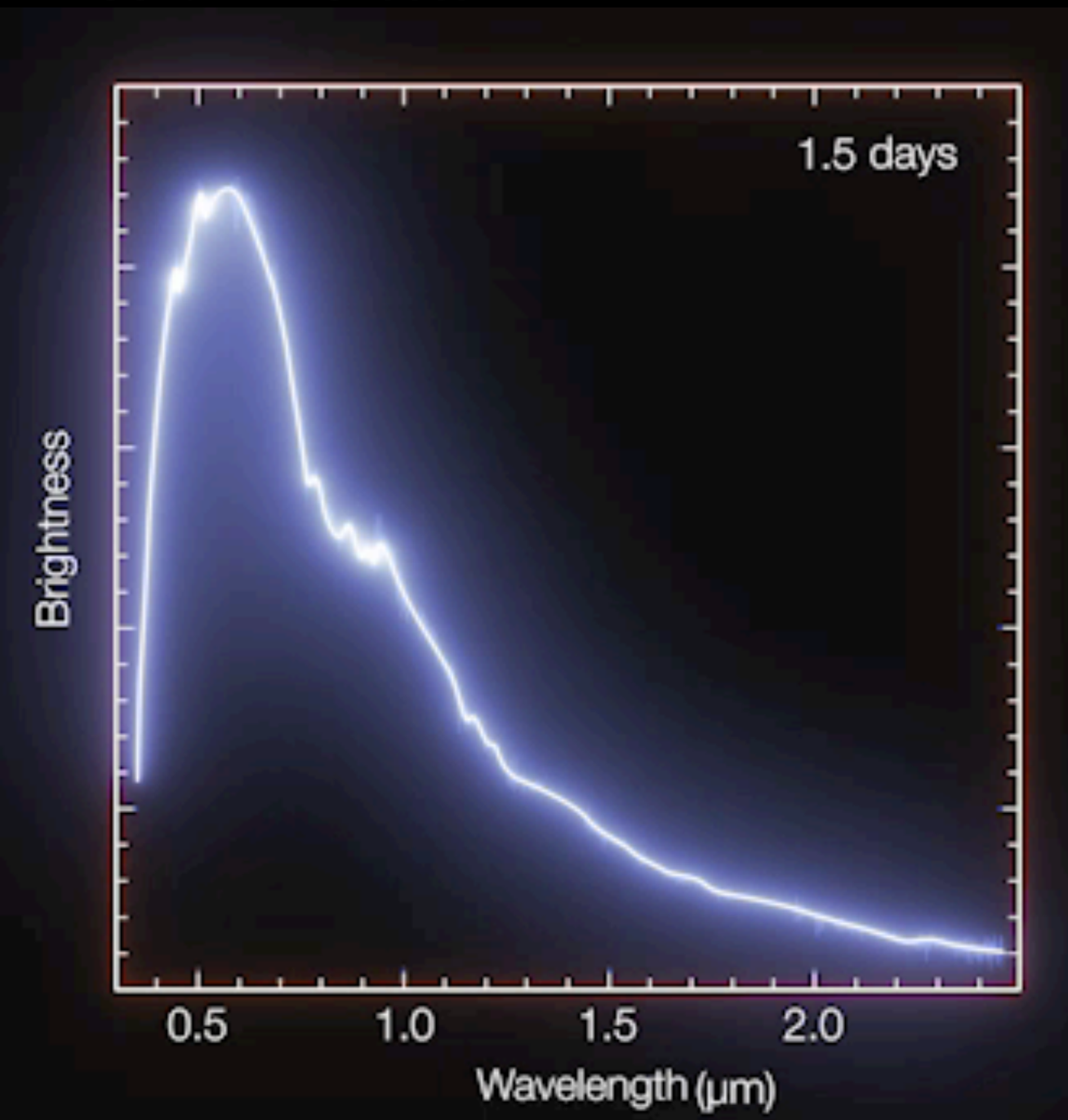

Credit: ESO/E. Pian et al./S. Smartt & ePESSTO/L. Calçada

First spectral identification of the kilonova emission

- the data revealed signatures of the radioactive decay of **r-process nucleosynthesis**
- BNS mergers **site for heavy elements production in the Universe!**

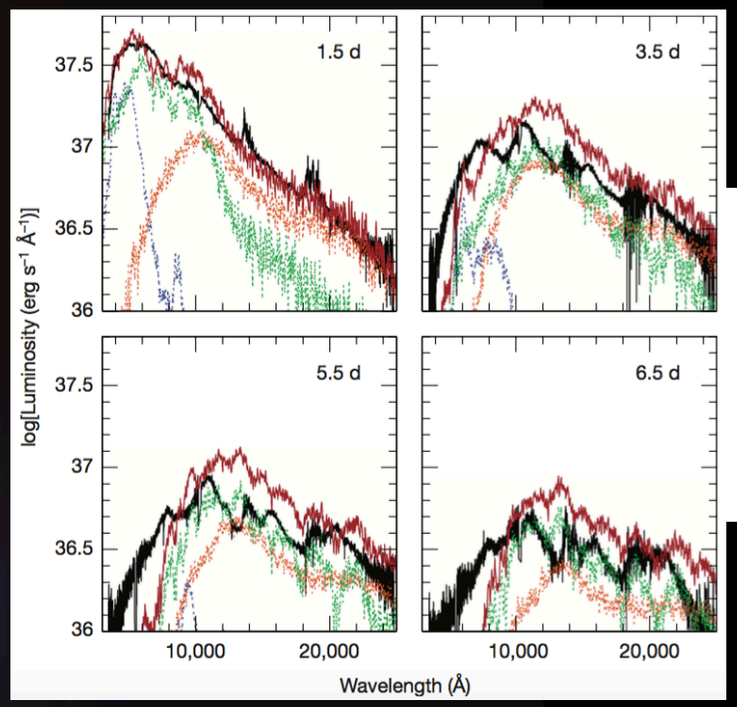

Pian et al. 2017, Nature

Tanaka et al. (2017)

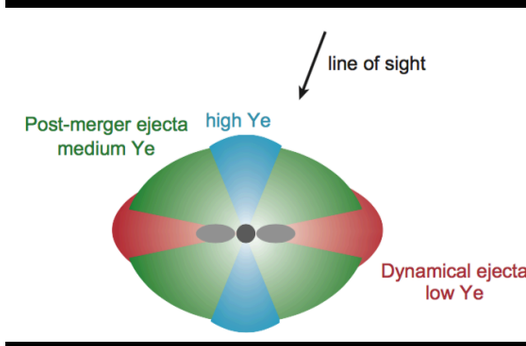

AT2017gfo Lightcurve

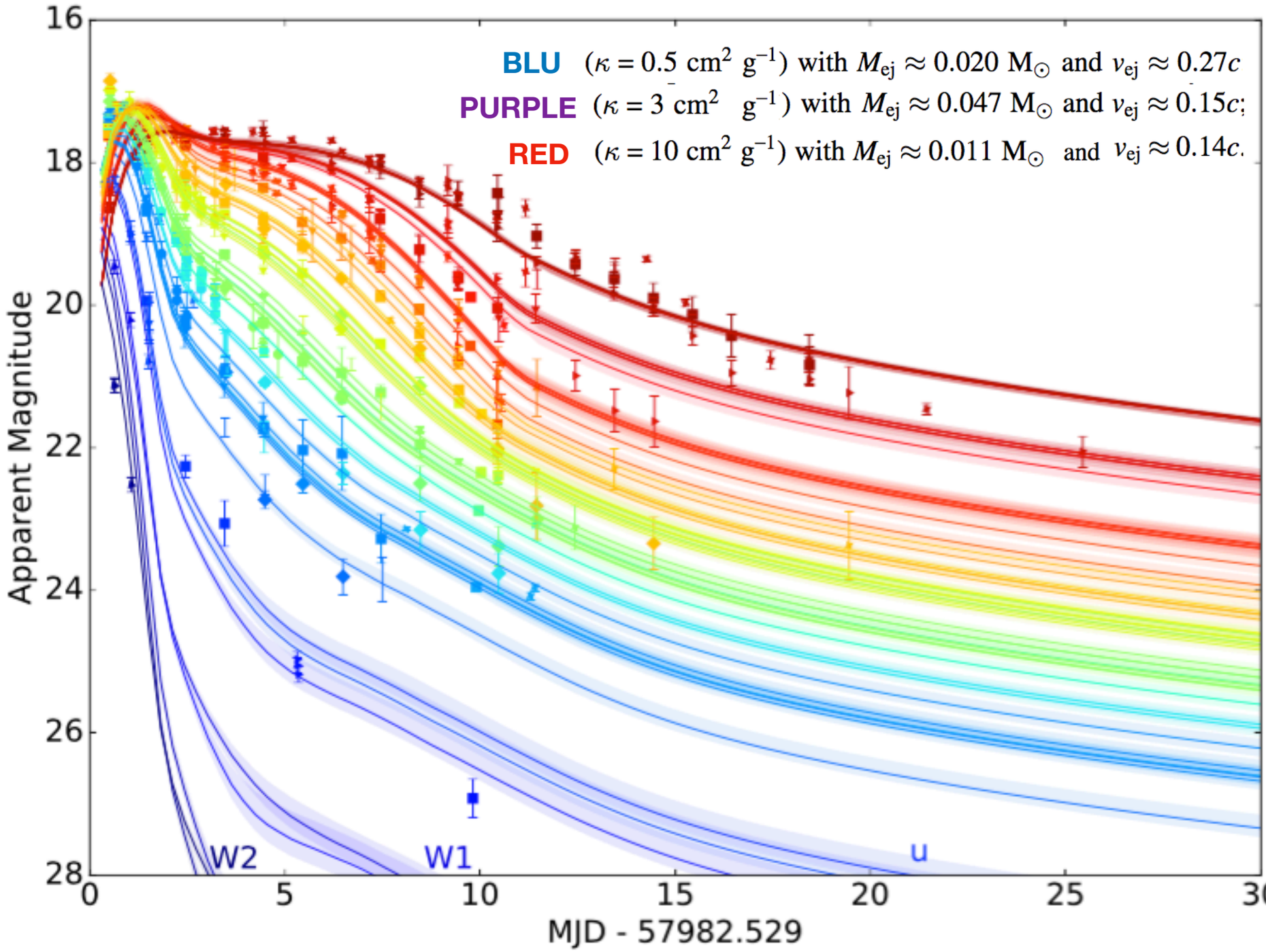

Villar et al. (2017)

Before AT2017gfo...

Kilonova Candidates

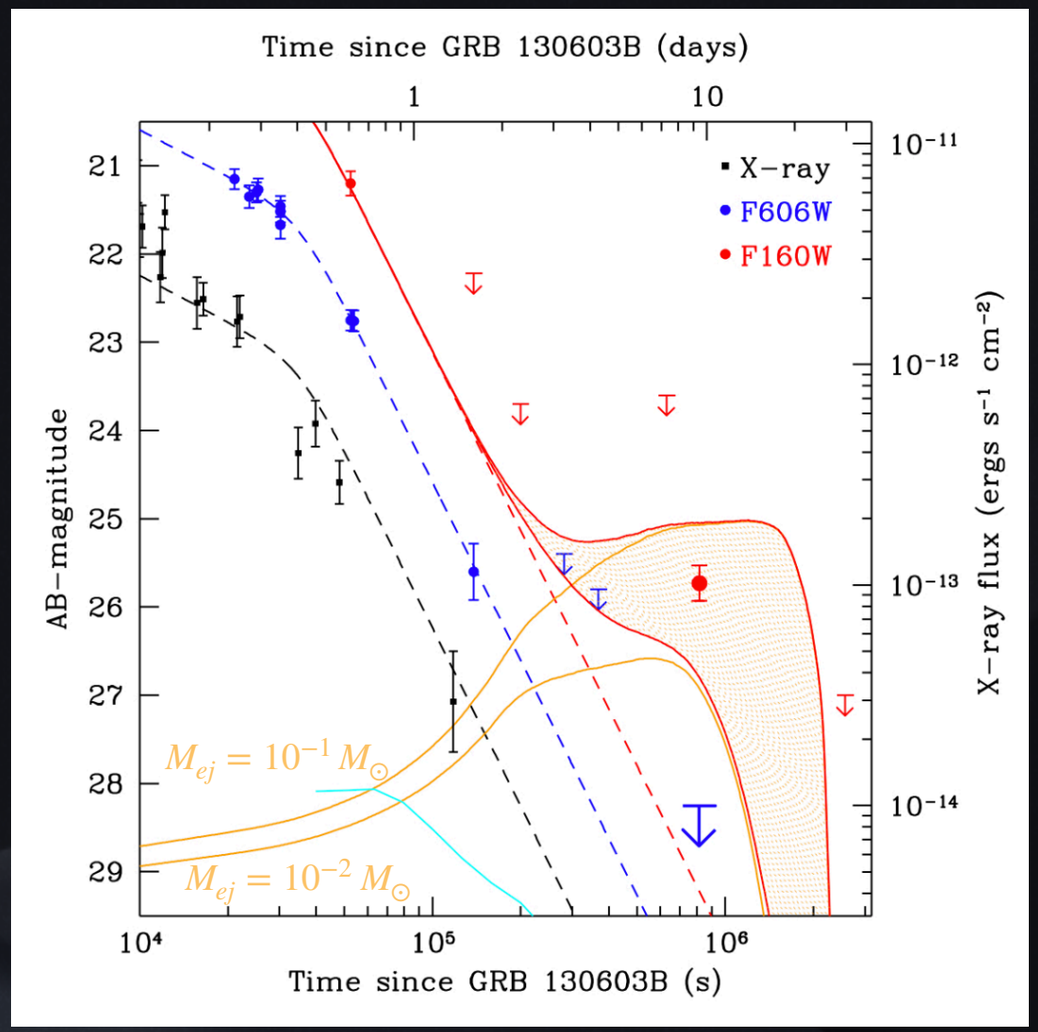

(Tanvir+2013)

Kilonova candidate found as NIR bump appearing late time during short GRB afterglow.

Most famous candidate GRB130603B (Tanvir+2013, Berger 2013)

Before AT2017gfo...

Kilonova Candidates

SN-less, Long GRB

($T_{90} \sim 100\,s$)

GRB	Ref.	Kilonova	M_{ej} ($M_\odot$)	X_{lan}	Redshift
170817A (GW170817)	1	Yes	$3.87^{+3.39}_{-1.44} \times 10^{-2}$	$2.71^{+8.60}_{-2.03} \times 10^{-4}$	0.0099
130603B	2, 3	Yes	$7.46^{+43.97}_{-7.29} \times 10^{-2}$	$5.36^{+64.63}_{-5.36} \times 10^{-3}$	0.356
050709	4, 5, 6, 7	Yes	$5.11^{+2.98}_{-2.13} \times 10^{-2}$	$4.49^{+49.60}_{-4.45} \times 10^{-5}$	0.161
060614	8, 9, 10	Yes	$7.73^{+1.90}_{-2.85} \times 10^{-2}$	$2.24^{+36.73}_{-2.23} \times 10^{-6}$	0.125
150101B	11, 12	Recently claimed by 12	$3.71^{+3.12}_{-1.56} \times 10^{-2}$	$4.19^{+889.60}_{-4.16} \times 10^{-7}$	0.134
140903A	13	No	–	–	0.351
050724A	14, 15	Recently claimed by 24	$1.24^{+39.99}_{-1.09} \times 10^{-2}$	$0.09^{+227.56}_{-0.09} \times 10^{-4}$	0.257
061201	16	Recently claimed by 24	$4.20^{+38.34}_{-2.91} \times 10^{-3}$	$0.07^{+361.50}_{-0.07} \times 10^{-4}$	0.111[a]
080905A	17, 18	Recently claimed by 24	$6.98^{+44.01}_{-4.58} \times 10^{-3}$	$1.41^{+200.38}_{-1.41} \times 10^{-4}$	0.1218
070724A	19, 20	No	–	–	0.457
160821B	21, 22	Recently claimed by 24	$1.74^{+6.97}_{-1.69} \times 10^{-1}$	$1.87^{+175.29}_{-1.87} \times 10^{-4}$	0.16
150424A	22, 23	Recently claimed by 24	$9.66^{+56.04}_{-9.45} \times 10^{-2}$	$0.15^{+188.15}_{-0.15} \times 10^{-4}$	0.30

Note: [a] This event has been associated to a galaxy at the redshift reported here or to the cluster Abell 995 at $z = 0.084$. Gompertz et al. (2018) employed for this event the latter value, while we choose the former in order to be more conservative.

References: (1) Abbott et al. (2017b), (2) Tanvir et al. (2013), (3) Berger et al. (2013), (4) Fox et al. (2005), (5) Hjorth et al. (2005), (6) Covino et al. (2006), (7) Jin et al. (2016), (8) Zhang et al. (2007), (9) Jin et al. (2015), (10) Yang et al. (2015), (11) Fong et al. (2016), (12) Troja et al. (2018a), (13) Troja et al. (2016), (14) Berger et al. (2005), (15) Malesani et al. (2007) (16) Stratta et al. (2007), (17) Nicuesa Guelbenzu et al. (2012), (18) Rowlinson et al. (2010), (19) Berger et al. (2009), (20) Kocevski et al. (2010), (21) Kasliwal et al. (2017c), (22) Jin et al. (2018), (23) Tanvir et al. (2015), (24) Rossi et al. (2019).

(Ascenzi+2019)

After AT2017gfo...

New Kilonovae - GRB 211211A

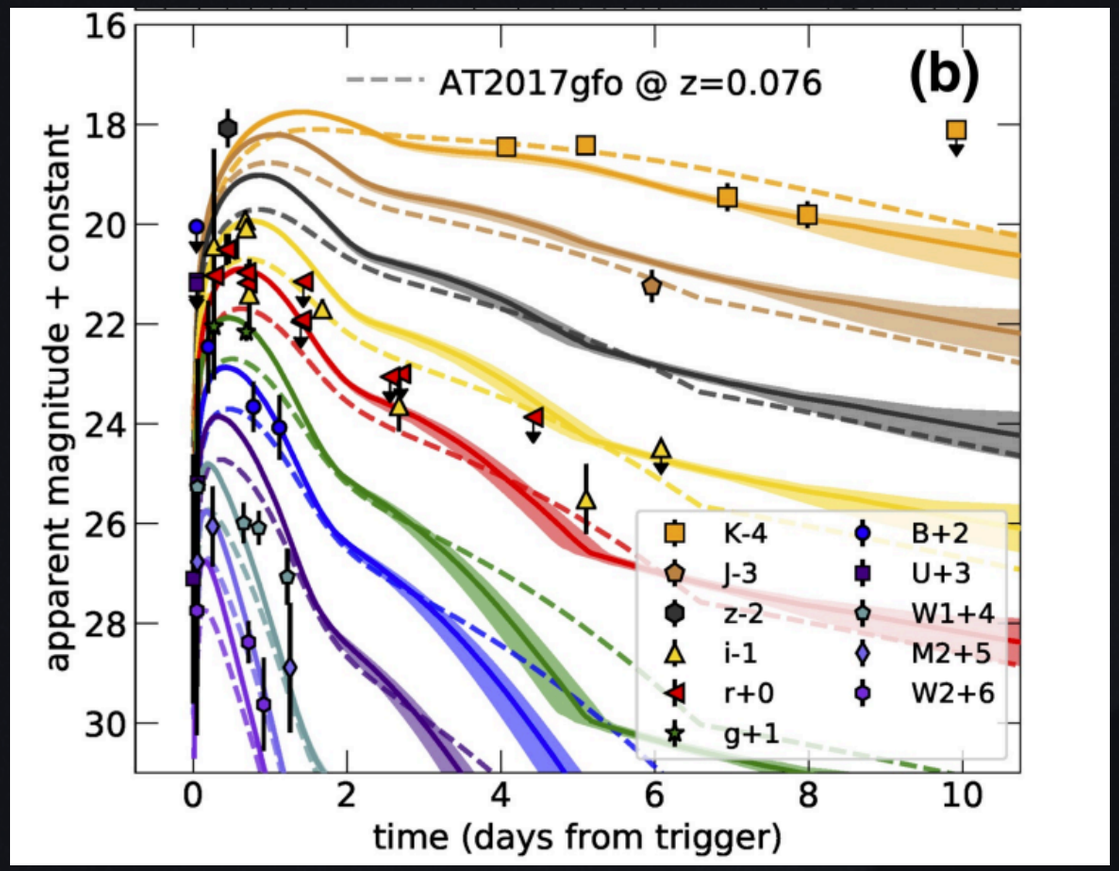

(Rastinejad+2022)

$$M_{ej,tot} = 0.047^{+0.026}_{-0.011}\, M_\odot$$

$M_{red} \sim 0.02\, M_\odot$ $v_{red} \sim 0.3c$

$M_{purple} \sim 0.01\, M_\odot$ $v_{purple} \sim 0.1c$

$T_{90} \sim 51.37\, s$

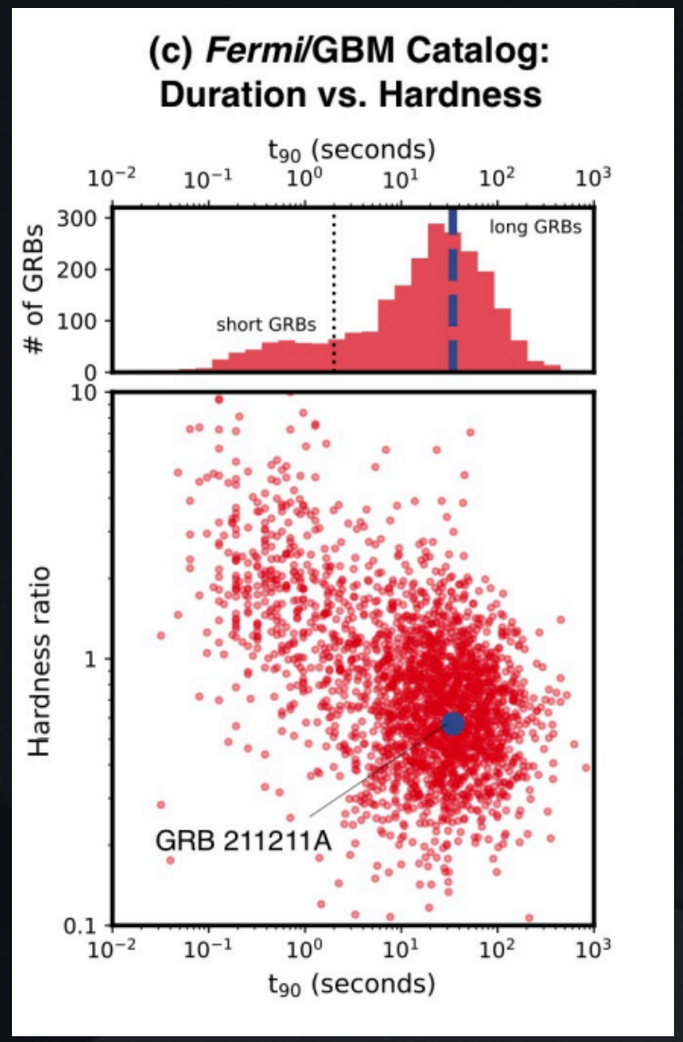

(Rastinejad+2022)

After AT2017gfo...

New Kilonovae - GRB 230307A

$T_{90} = 35\ s$ another Long

(Levan+2023)

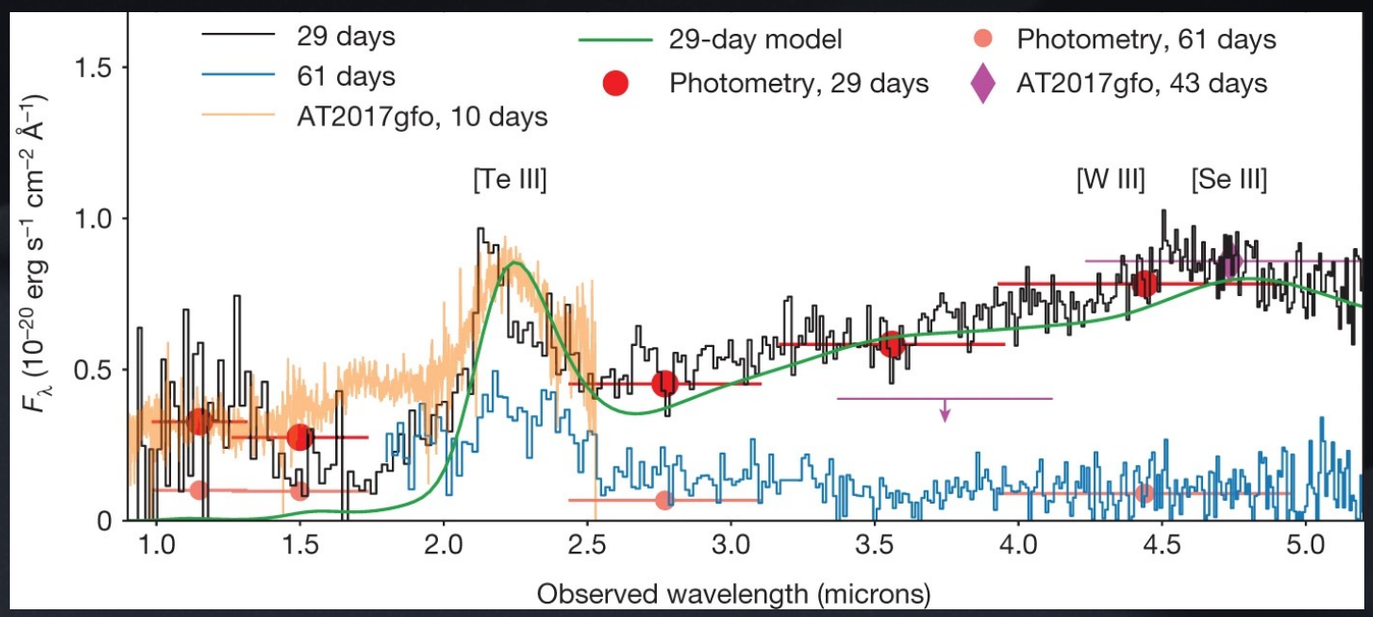

(Levan+2023)

(Solid lines = Afterglow
shaded+hatched region kilonova)

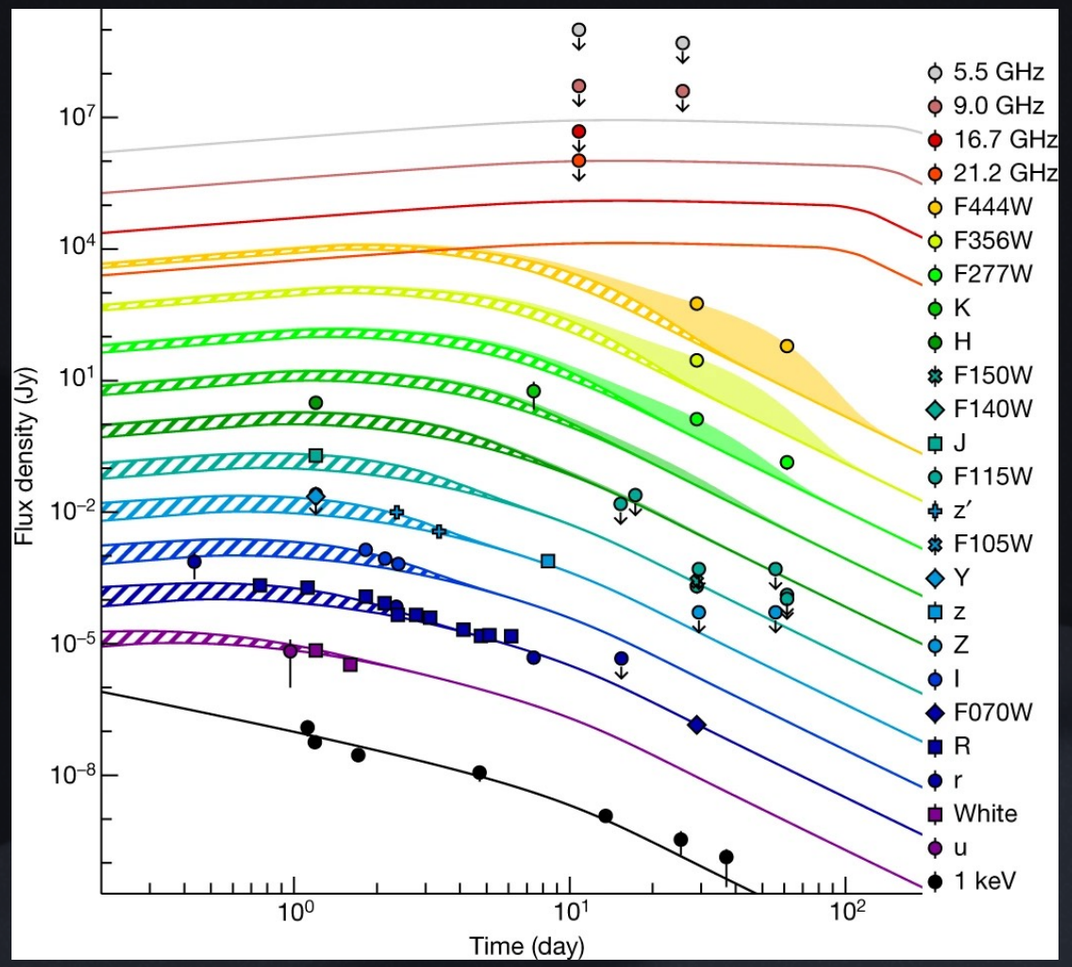

(Yang+2024)

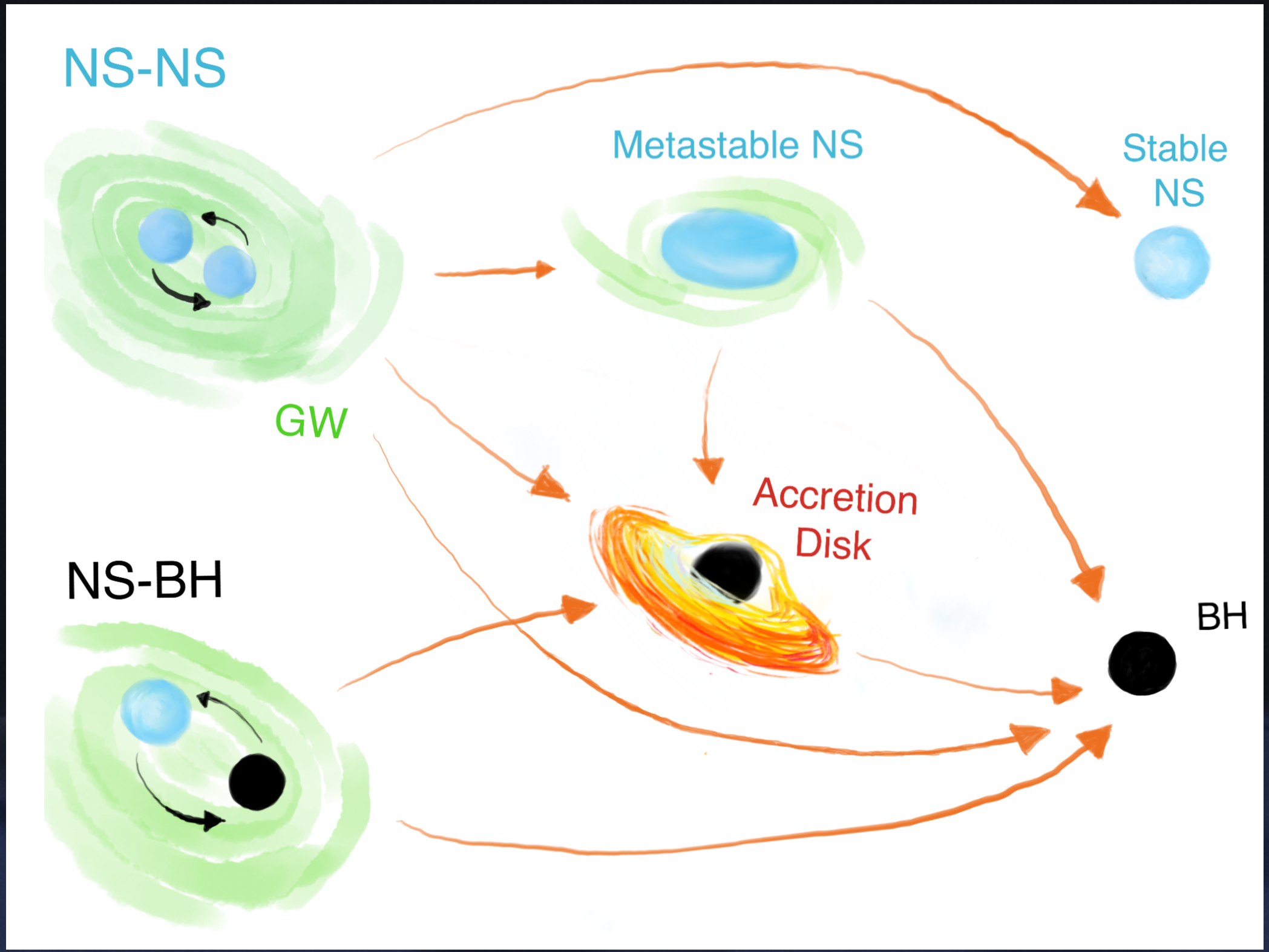

Ascenzi et al. 2021

Binary Neutron Star Merger

Electron Fraction

$$Y_e = \frac{\text{\# of electrons}}{\text{\# of nucleons}}$$

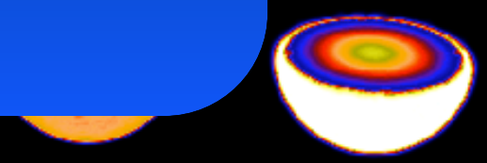

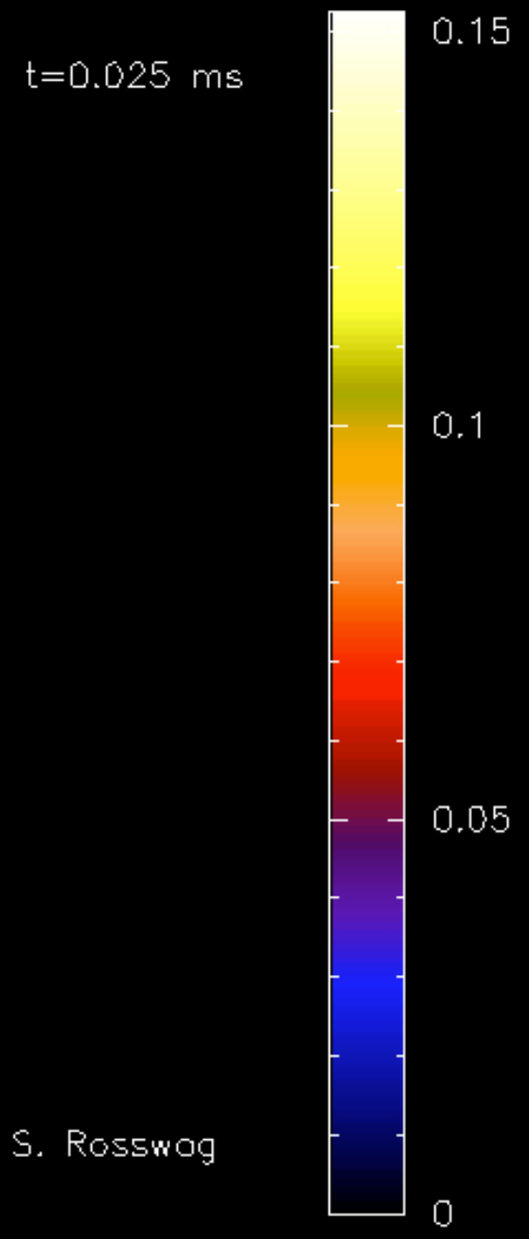

R-Process Nucleosynthesis

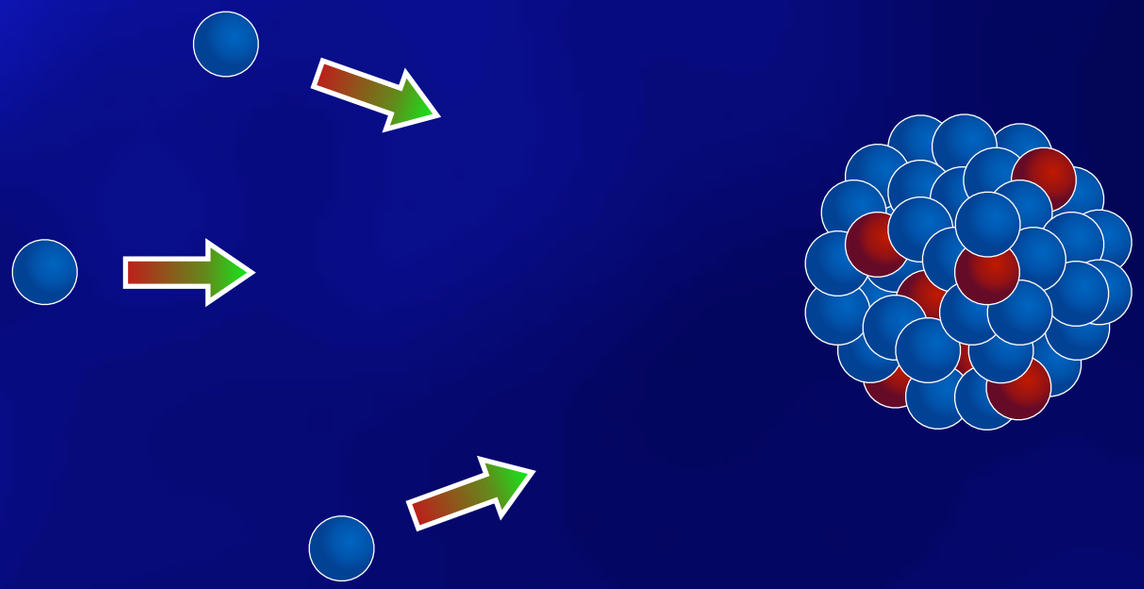

R-Process Nucleosynthesis

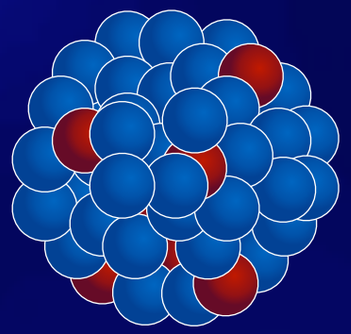

R-Process Nucleosynthesis

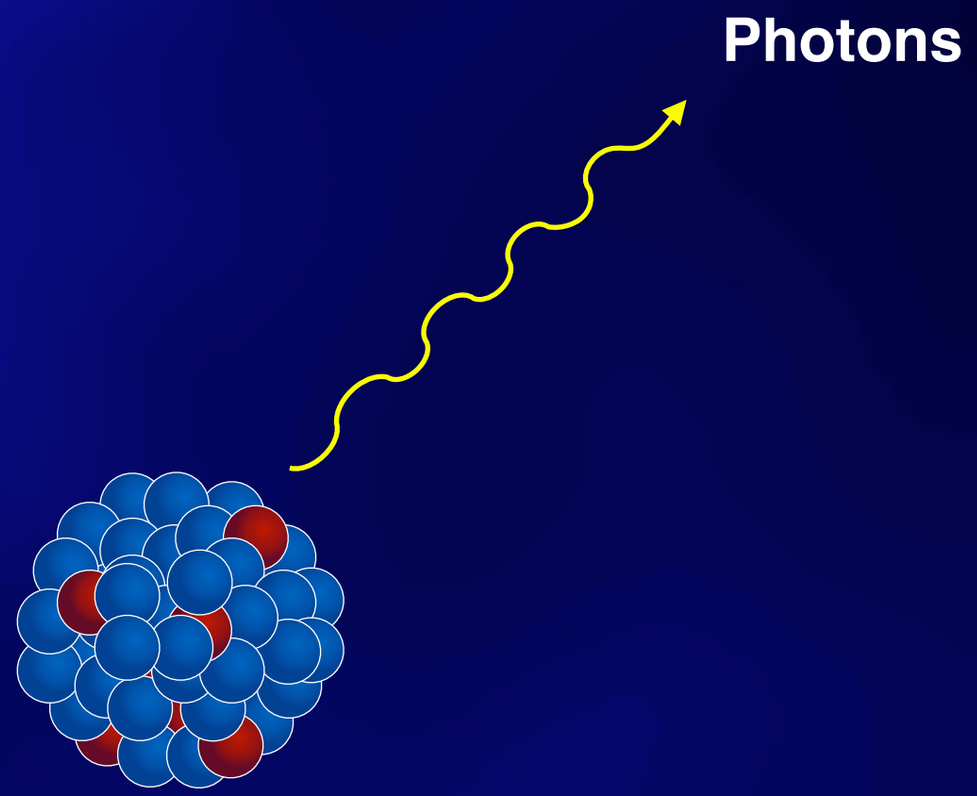

R-Process Nucleosynthesis

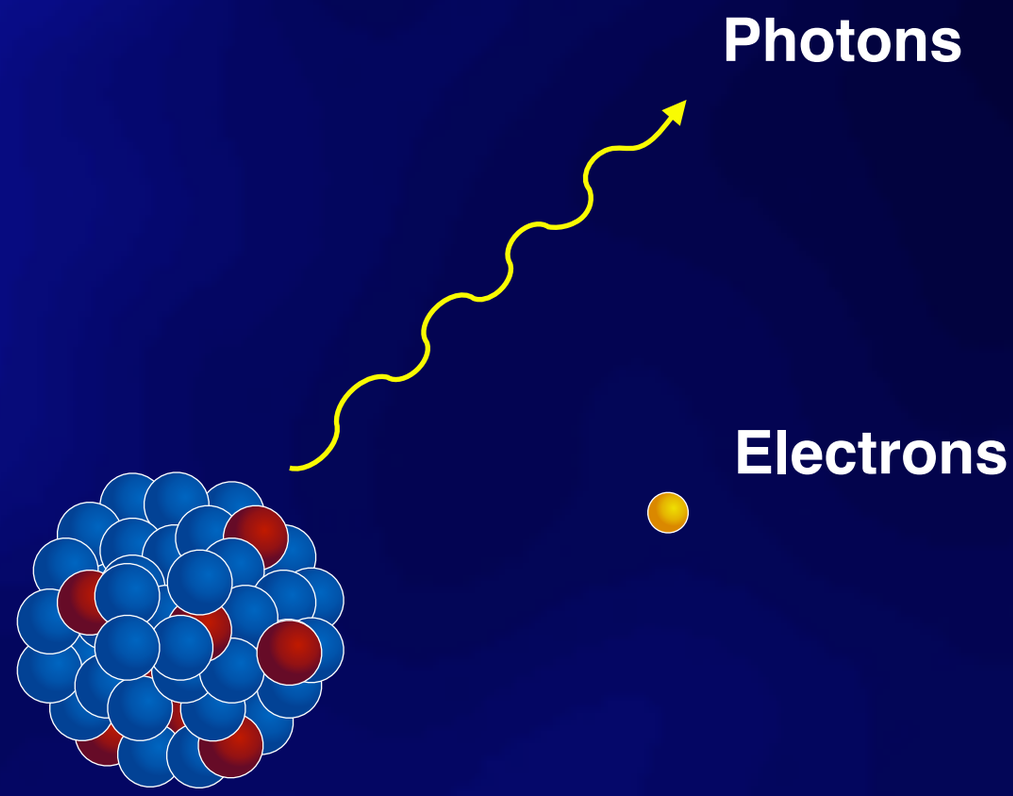

R-Process Nucleosynthesis

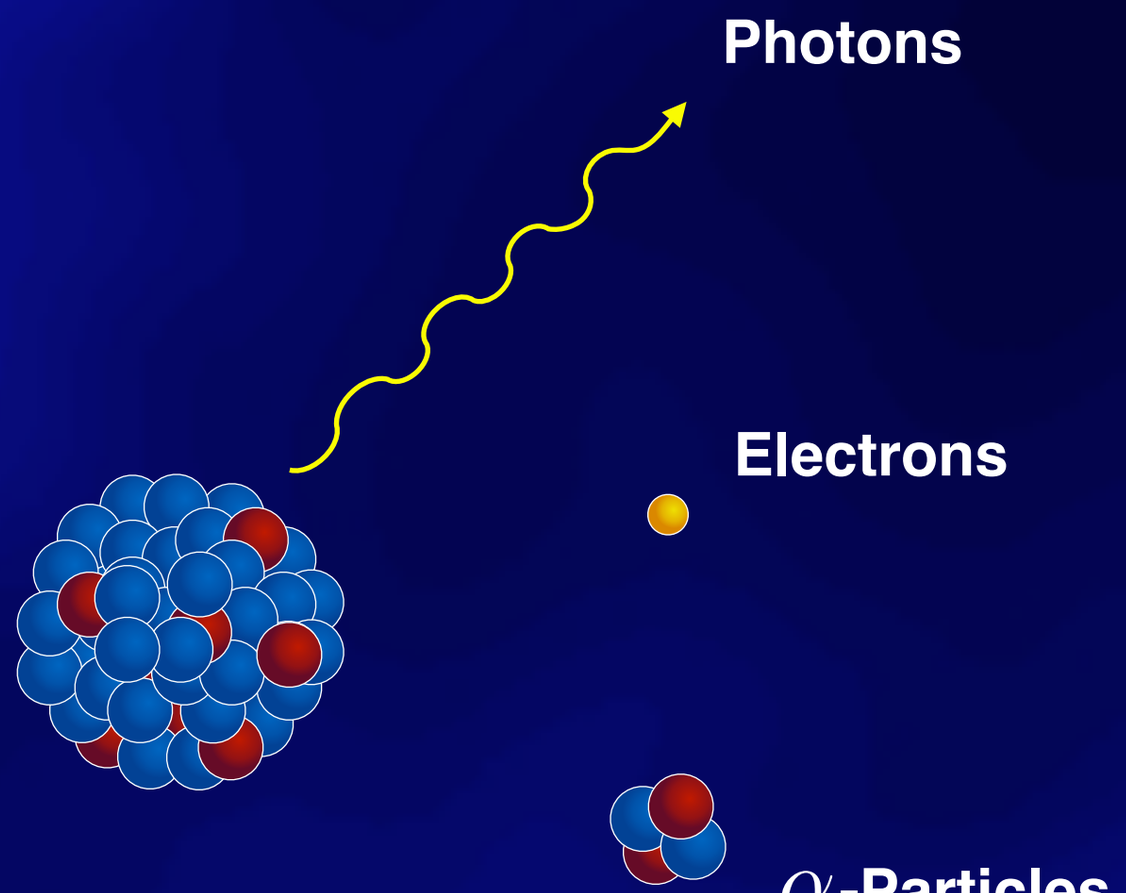

R-Process Nucleosynthesis

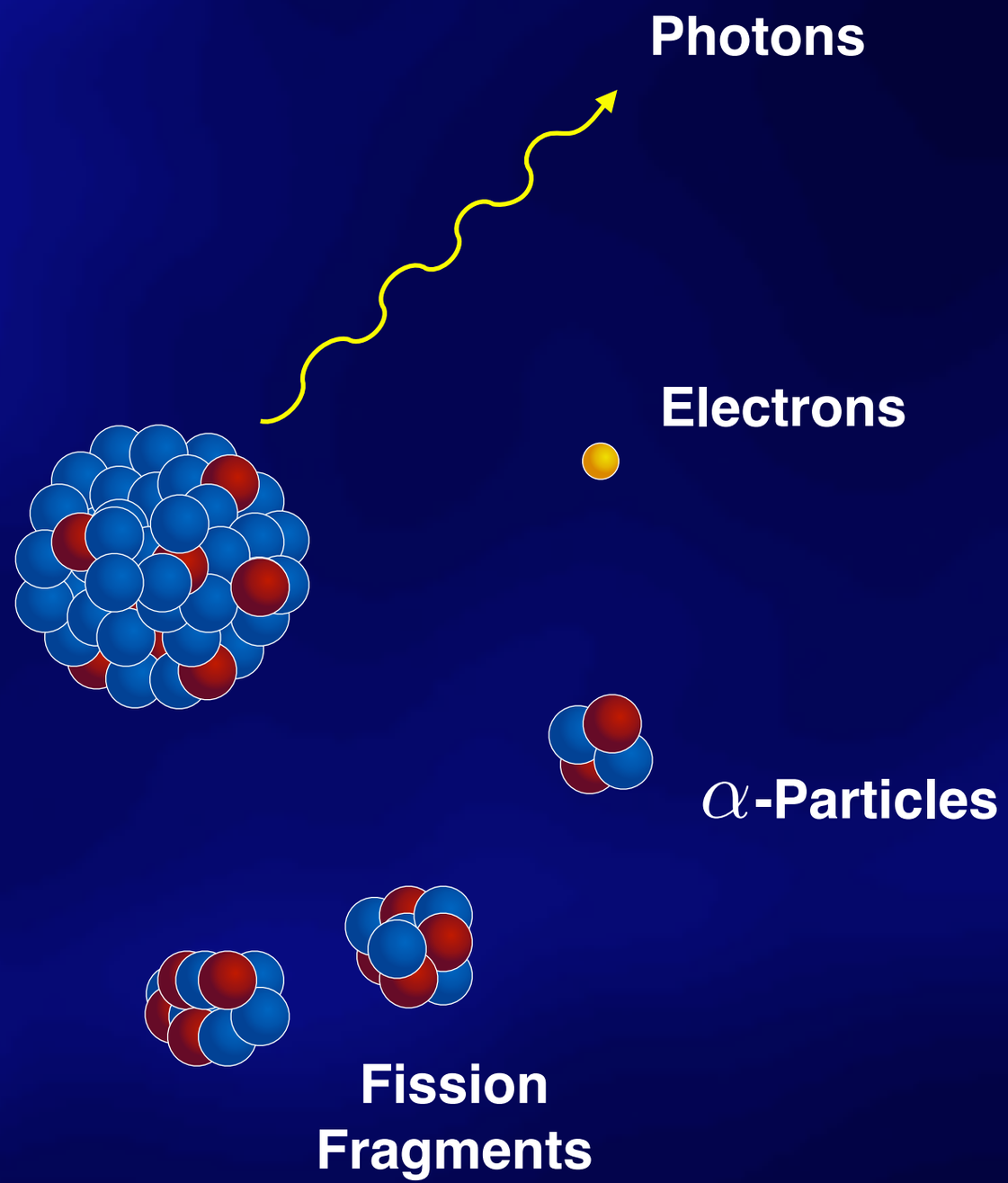

ACME
Astrophysics Centre for Multimessenger studies in Europe

Thermal Optical-NIR Emission (Kilonova)

$\vec{v}$

Unbound expanding matter heated by radioactive decays

Remnant + Accretion Disk

Table 1 Timeline of major developments in kilonova research

1974	Lattimer and Schramm: r-process from BH–NS mergers
1975	Hulse and Taylor: discovery of binary pulsar system PSR 1913 + 16
1982	Symbalisty and Schramm: r-process from NS–NS mergers
1989	Eichler et al.: GRBs from NS–NS mergers
1994	Davies et al.: first numerical simulation of mass ejection from NS–NS mergers
1998	Li and Paczyński: first kilonova model, with parameterized heating
1999	Freiburghaus et al.: NS–NS dynamical ejecta ⇒ r-process abundances
2005	Kulkarni: kilonova powered by free neutron-decay (“macronova”), central engine
2009	Perley et al.: optical kilonova candidate following GRB 080503 (Fig. 9)
2010	Metzger et al., Roberts et al., Goriely et al.: kilonova powered by r-process heating
2013	Barnes and Kasen, Tanaka and Hotokezaka: La/Ac opacities ⇒ NIR spectral peak
2013	Tanvir et al., Berger et al.: NIR kilonova candidate following GRB 130603B
2013	Yu, Zhang, Gao: magnetar-boosted kilonova (“merger-nova”)
2014	Metzger and Fernandez, Kasen et al.: blue kilonova from post-merger remnant disk winds

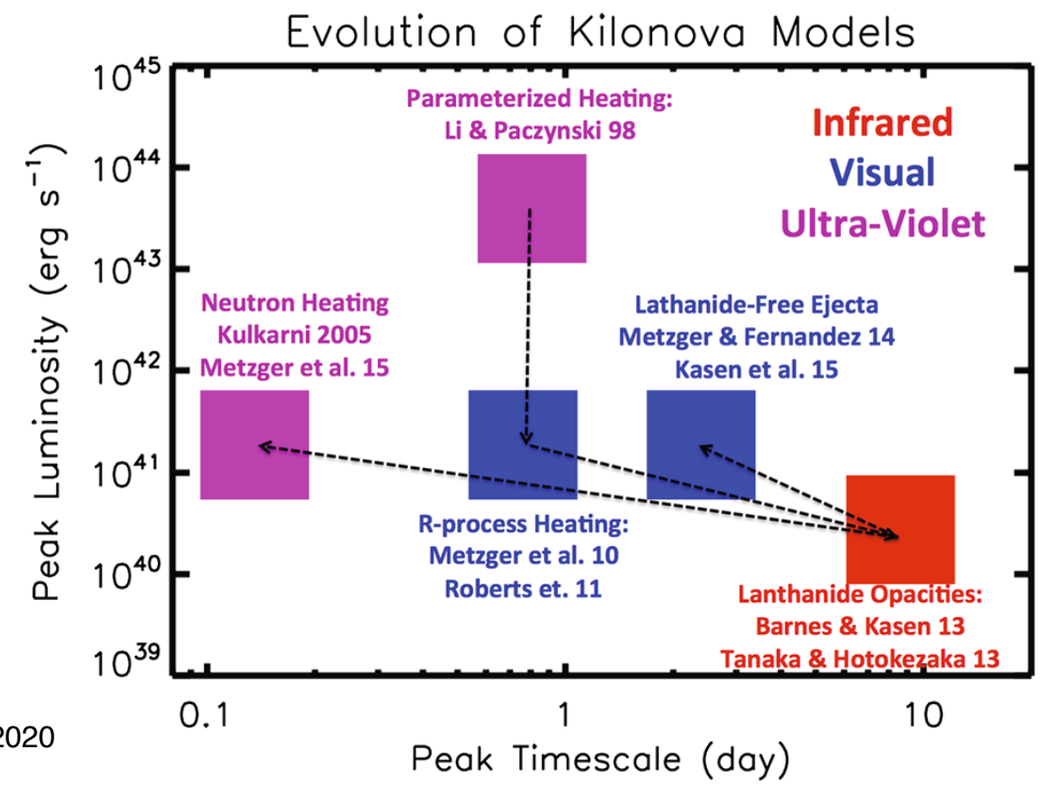

Metzger 2020

Why are they interesting?

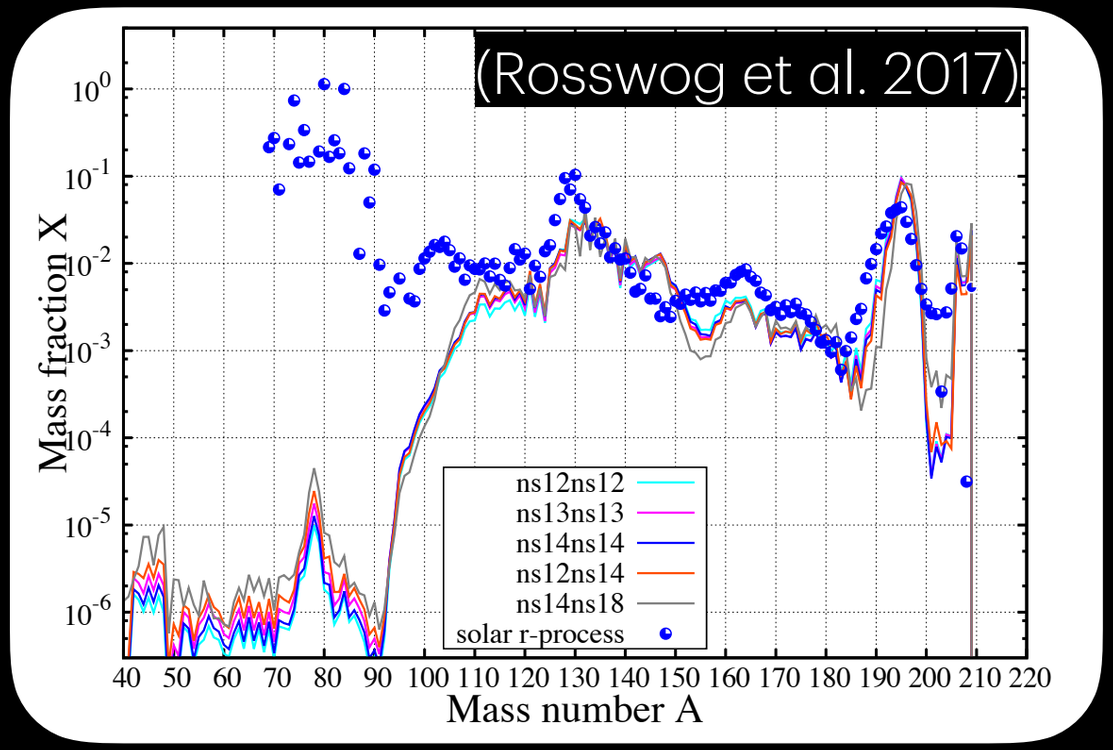

R-process nucleosynthesis

Quasi-Isotropic counterparts of GWs from BNS mergers

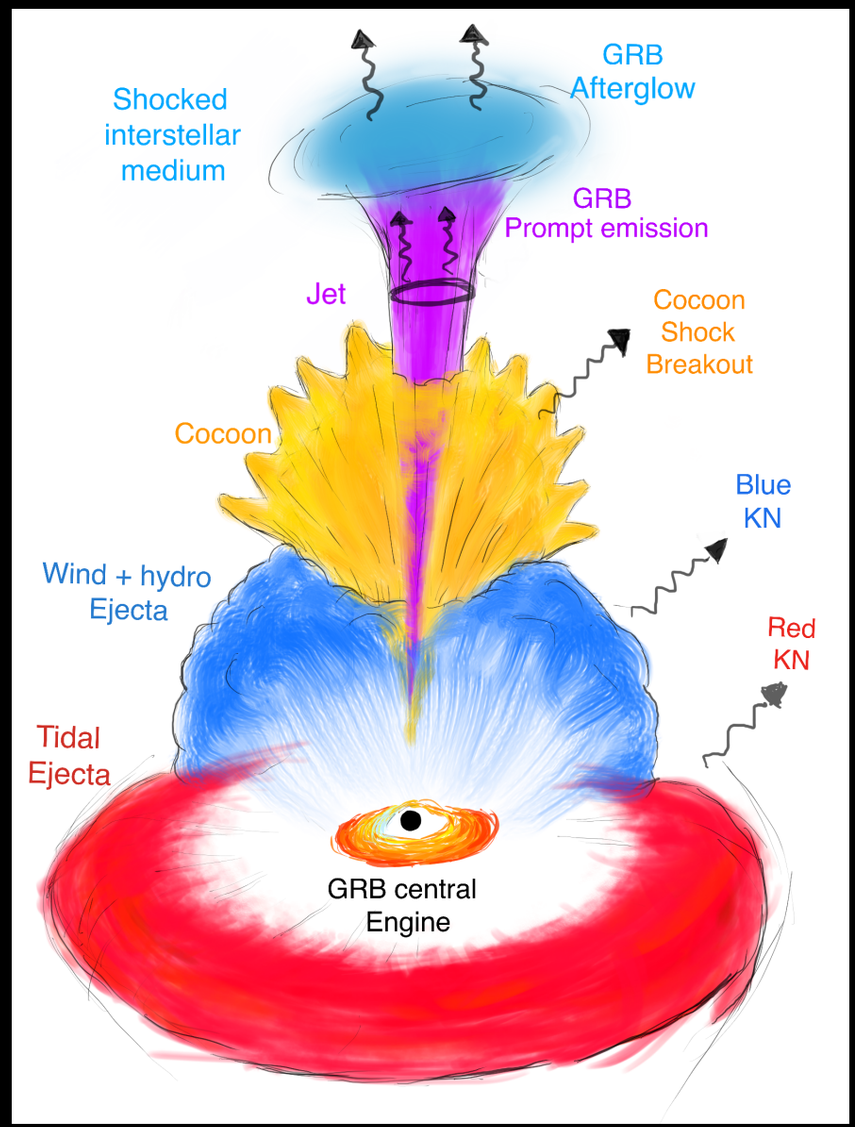

(Ascenzi et al. 2021)

Let's build a toy kilonova model

(Adapted from D. Kasen notes that follows Arnett 1980, 1982)

Heating

$$\frac{d\mathscr{E}_{int}}{dt} = -P\frac{dV}{dt} + \dot{Q}(t) - L(t)$$

Work (Adiabatic cooling)

Luminosity

Assumptions:

1. Spherical, 1-zone model
2. Free-expansion: $R(t) = \mathrm{v}t + R_0$
3. Radiation energy >> gas energy: $E = \mathscr{E}_{int}/V = aT^4,\ P = aT^4/3$
4. Rad. Cooling described by diffusion: $L(r) = -4\pi r^2 \frac{c}{3k\rho}\frac{\partial E}{\partial r}$
5. Constant opacity k

Step 1: timescale of photon escape

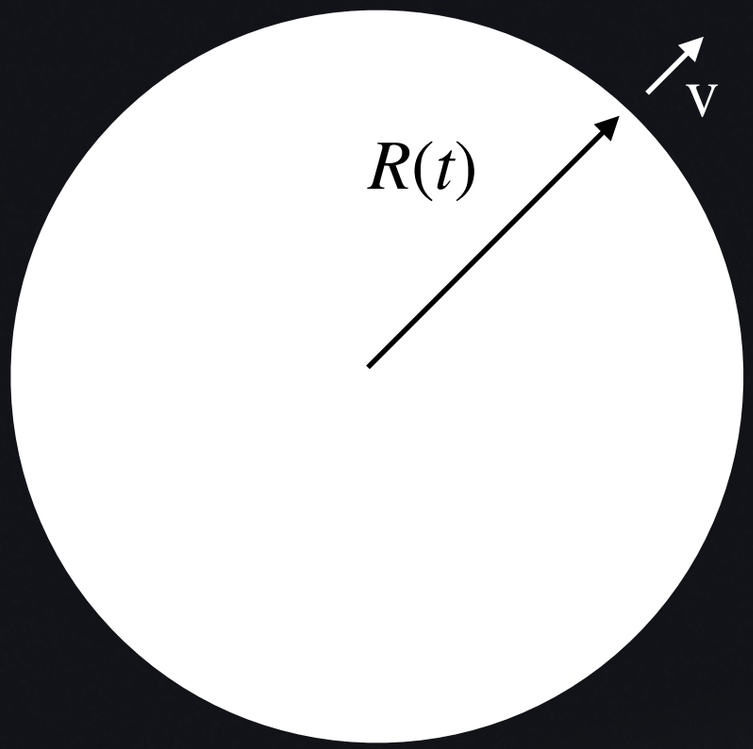

$$\tau = \rho k R$$

$$t_{diff} = \frac{R}{c}\tau = \frac{\rho k R^2}{c} \simeq \frac{3Mk}{4\pi c v t}$$

$$t_{diff}(t) = t \quad \Rightarrow \quad t_{rad} = \sqrt{\frac{3Mk}{4\pi v c}}$$

Step 2: Luminosity

$$L(R) = -4\pi R^2 \frac{c}{3\rho k}\frac{\partial E}{\partial r}(r = R)$$

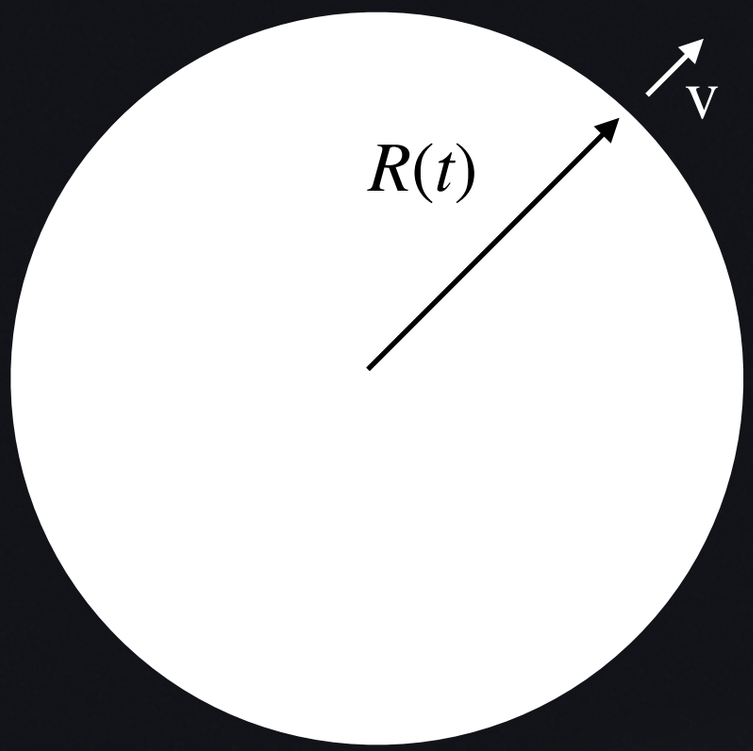

$$\frac{\partial E}{\partial r} \sim -\frac{\mathscr{E}_{int}}{VR}$$

$$L(R) = 4\pi R \frac{c}{3Mk}\mathscr{E}_{int} = \frac{\mathscr{E}_{int}(t)}{t_{rad}^2}(t + t_0) \qquad t_0 = R_0/v$$

Step 2: Luminosity equation

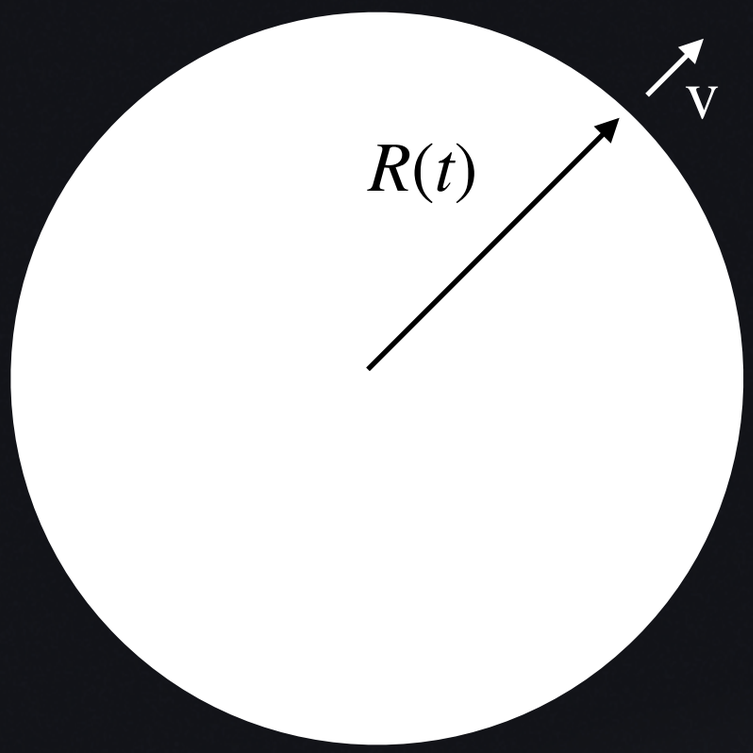

$$\frac{d\mathscr{E}_{int}}{dt} = -P\frac{dV}{dt} + \dot{Q}(t) - L(t)$$

$$P\frac{dV}{dt} = \frac{1}{3}\frac{\mathscr{E}_{int}}{V}\frac{dV}{dt} = \frac{\mathscr{E}_{int}}{R}\frac{dR}{dt} = \frac{\mathscr{E}_{int}}{t+t_0}$$

$$\frac{d\mathscr{E}_{int}}{dt} = \frac{d}{dt}\left(\frac{Lt_{rad}^2}{t+t_0}\right) = \frac{t_{rad}^2}{t+t_0}\frac{dL}{dt} - \frac{\mathscr{E}_{int}}{t+t_0}$$

$$\frac{dL}{dt} = \frac{t+t_0}{t_{rad}^2}\left[\dot{Q}(t) - L(t)\right]$$

Step 2: Solving Luminosity equation

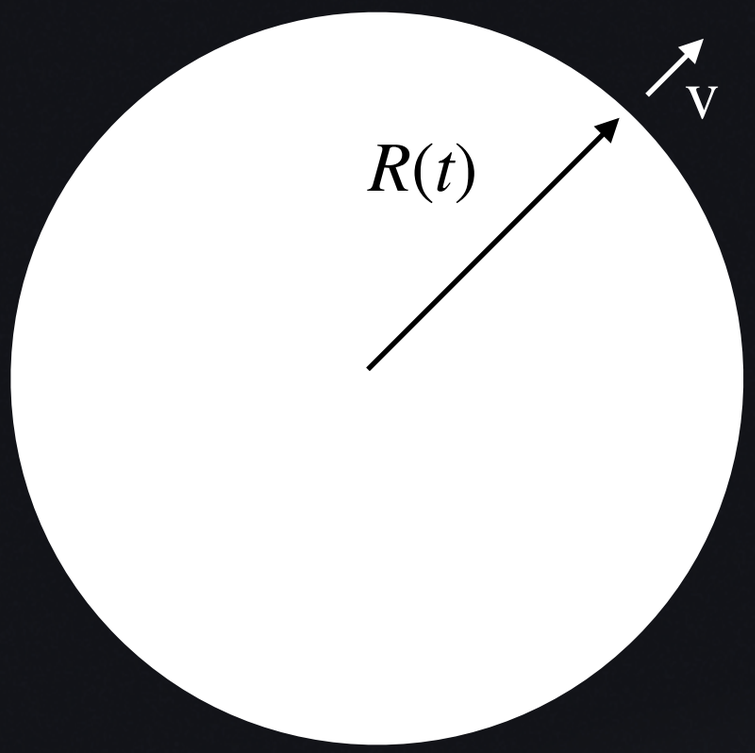

$$\frac{dL}{dt} = \frac{t + t_0}{t_{rad}^2}\left[\dot{Q}(t) - L(t)\right]$$

Using the integrating factor

$$\exp\left(\frac{t^2}{2t_{rad}^2}\right)$$

$$t \gg t_0$$

$$L(t) = \exp\left(-\frac{t^2}{2t_{rad}^2}\right)\left[\frac{\mathscr{E}_0 R_0}{\mathrm{v} t_{rad}^2} + \int_0^t \dot{Q}(t')\left(\frac{t'}{t_{rad}^2}\right)\exp\left(\frac{t'^2}{2t_{rad}^2}\right)dt'\right]$$

Kilonova: Main Ingredients

k ← Opacity

m_{ej} ← Mass of the Ejecta

v_{ej} ← Velocity of the Ejecta

$$t_{peak} \simeq 4.9\,days \left(\frac{k}{10\,cm^2/g}\frac{m_{ej}}{0.01\,M_\odot}\frac{0.1\,c}{v_{ej}}\right)^{1/2}$$

$$L_{peak} \simeq 2.5\times10^{40}\,\frac{erg}{s}\left(\frac{v_{ej}}{0.1\,c}\frac{10\,cm^2/g}{k}\right)^{0.65}\left(\frac{m_{ej}}{0.01\,M_\odot}\right)^{0.35} \bigstar$$

$$T_{peak} = 2200\,K\left(\frac{k}{10\,cm^2/g}\right)^{-0.41}\left(\frac{v}{0.1\,c}\right)^{-0.09}\left(\frac{m_{ej}}{0.01\,M_\odot}\right)^{-0.16} \bigstar$$

(Grossman et al. 2014)

★ Assume: PL index for r-process decay $a = 1.3$

Blue & Red Kilonova

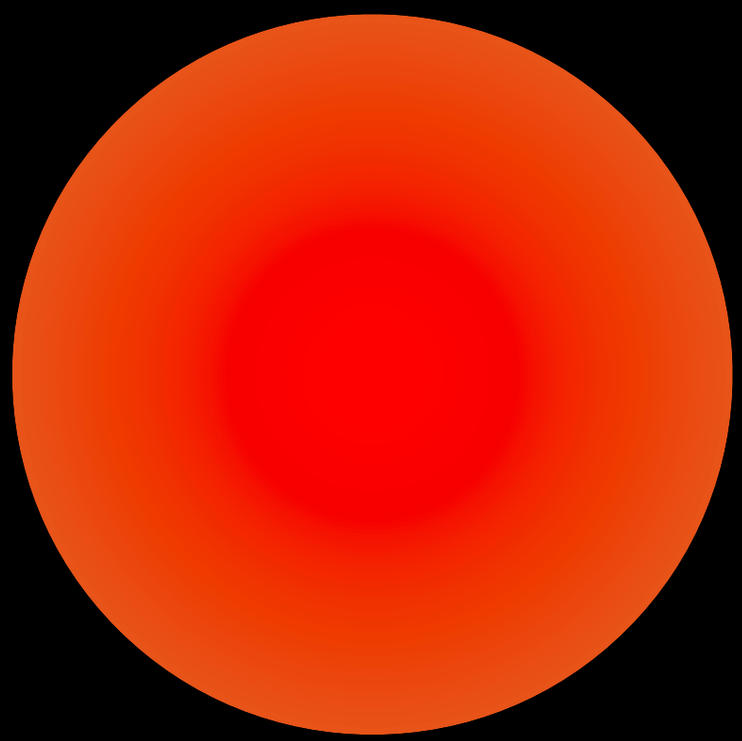

Red Kilonova

t_{peak}	Days- 1 week after the merger
L_{peak}	$10^{41}\ erg/s$
Spectral Range:	Optical Red/ NIR

Blue Kilonova

t_{peak}	1-day after the merger
L_{peak}	$\gtrsim 10^{41}\ erg/s$
Spectral Range:	Optical

Going deeper into the problem...

- R-process nucleosynthesis
- Heating Rates
- Thermalization efficiency
- Opacity and composition
- Multi-ejecta Components

R-Process Nucleosynthesis

Basic Reactions

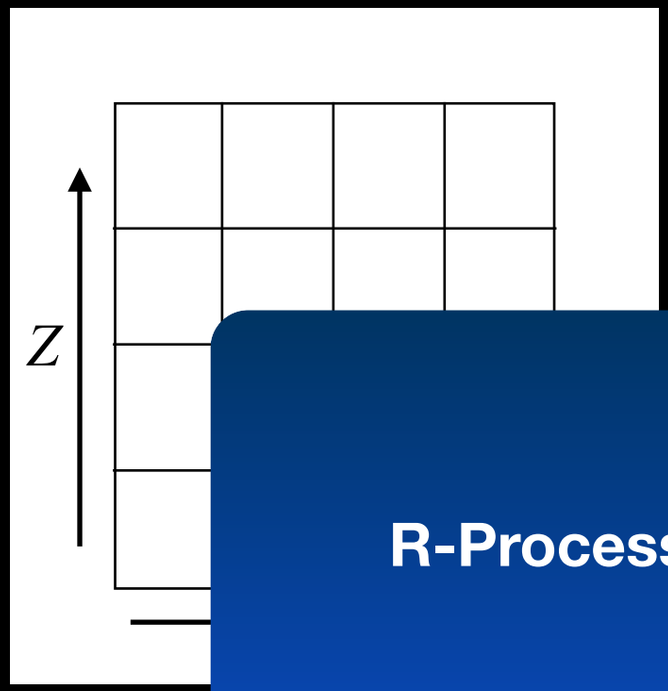

Neutron Capture

R-Process

Neutron capture timescale smaller than beta decay timescale

S-Process

Beta decay timescale smaller than neutron capture timescale

# of Neutrons

(Z, N)

Atomic Number
(# of protons)

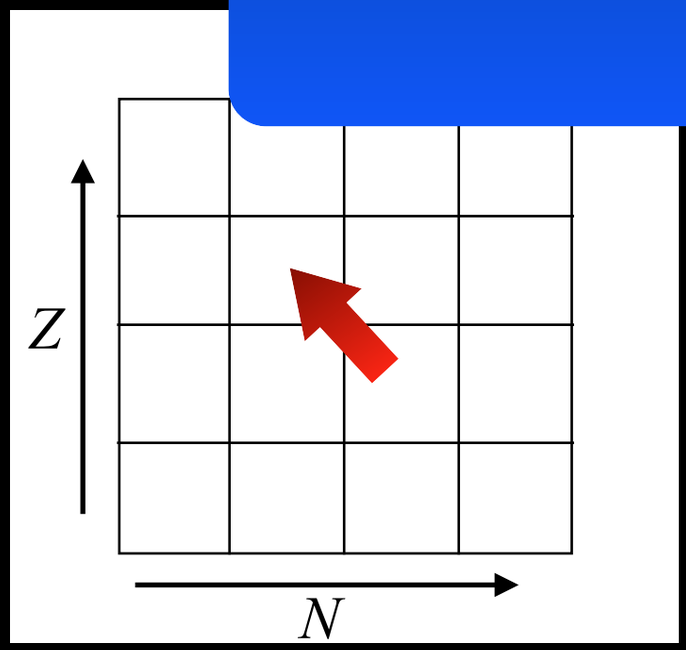

Beta Decay

$$(Z, N) \rightarrow (Z + 1, N - 1) + e^{-} + \bar{\nu}_e$$

R-processes: a qualitative description

Chart of Nuclides

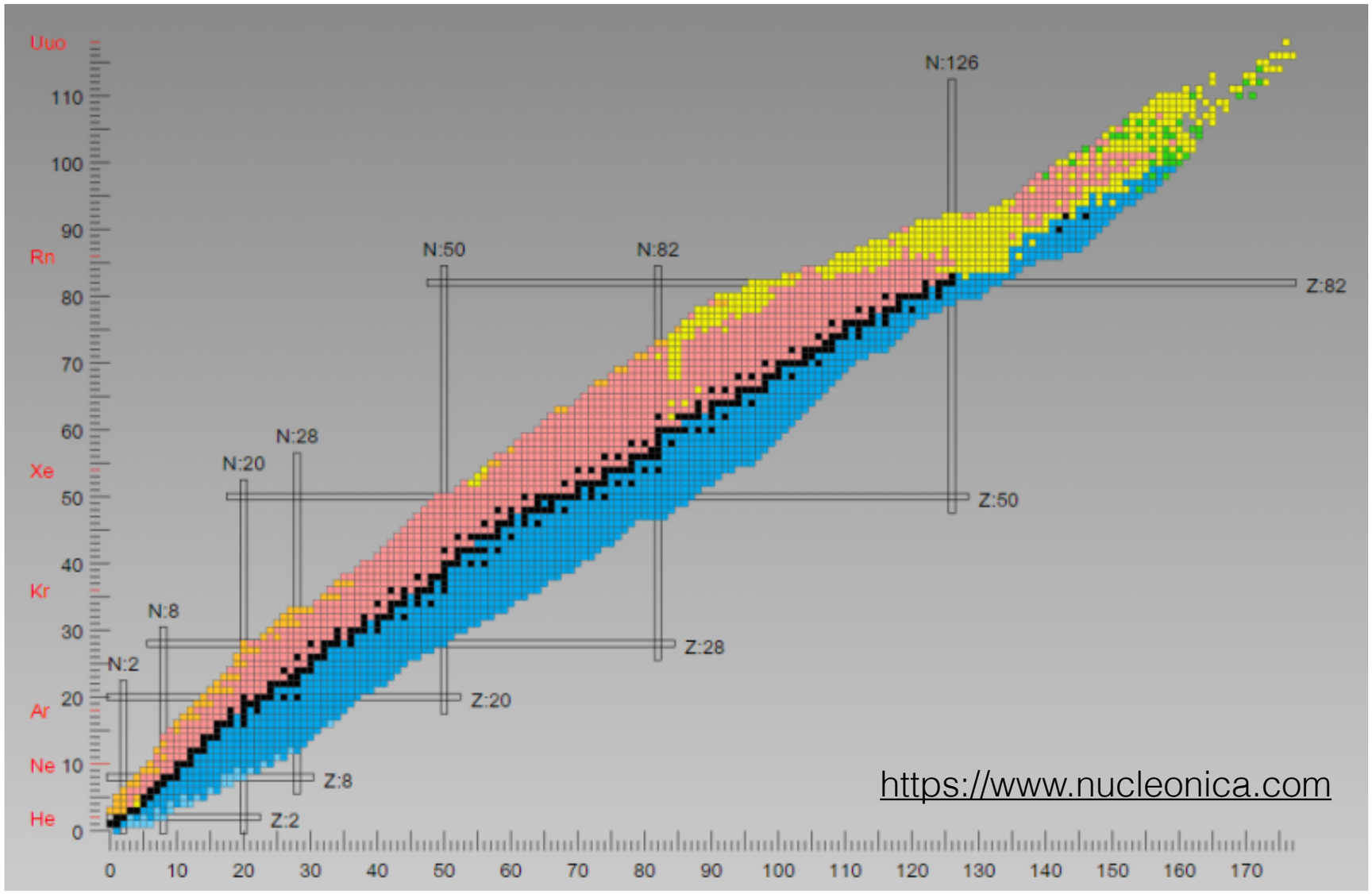

Proton Number

Neutron Number

R-processes: a qualitative description

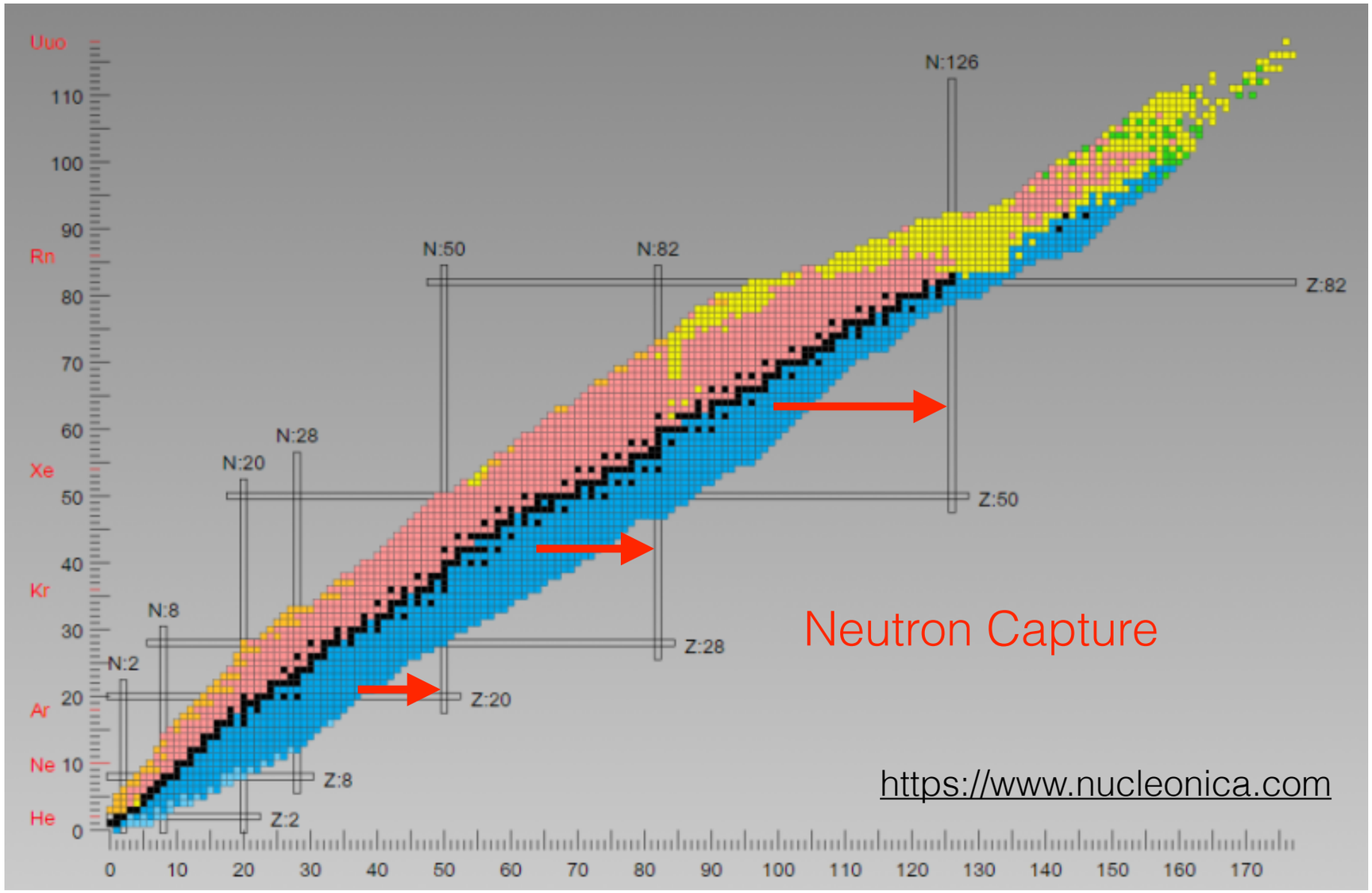

R-processes: a qualitative description

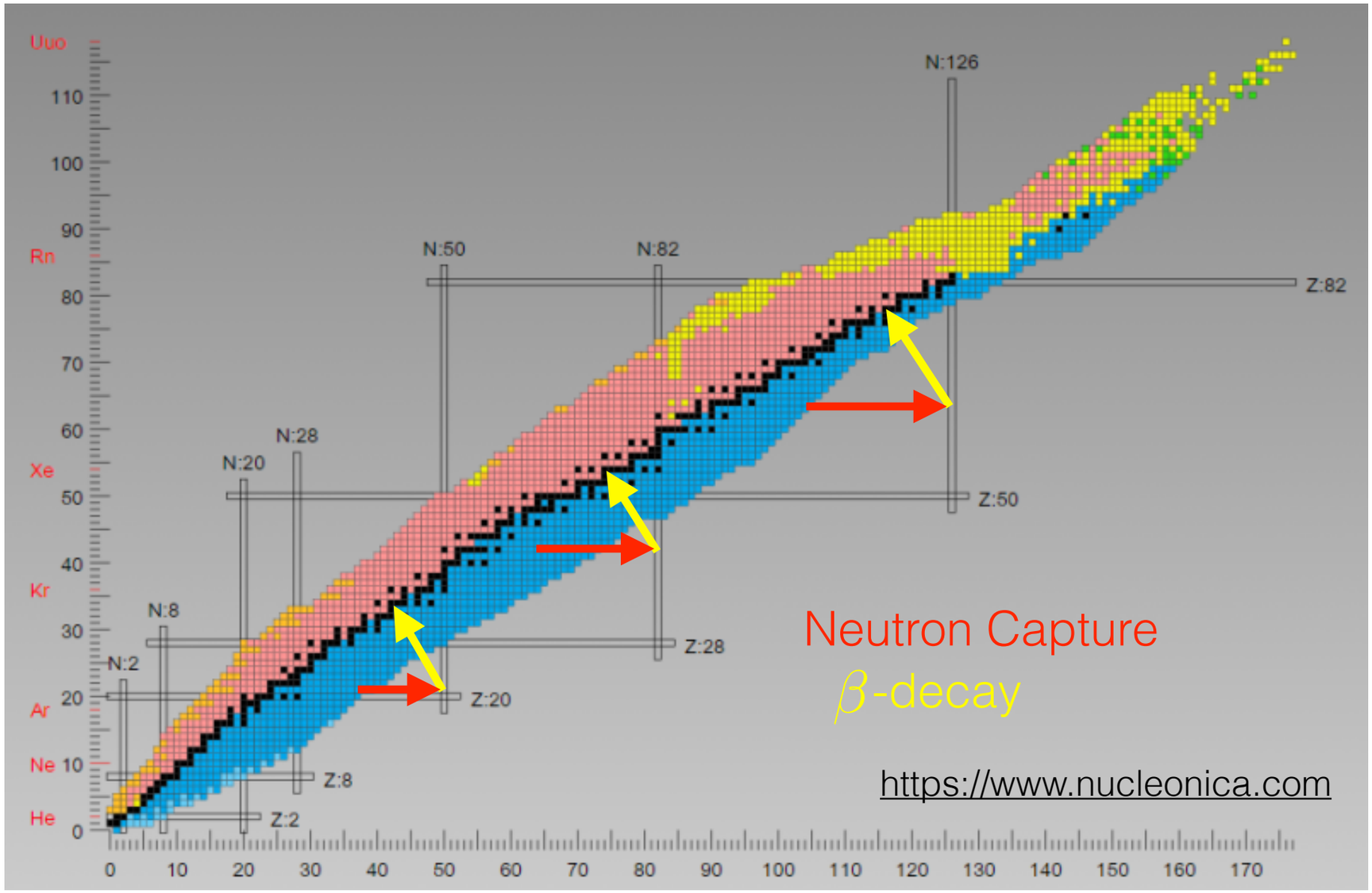

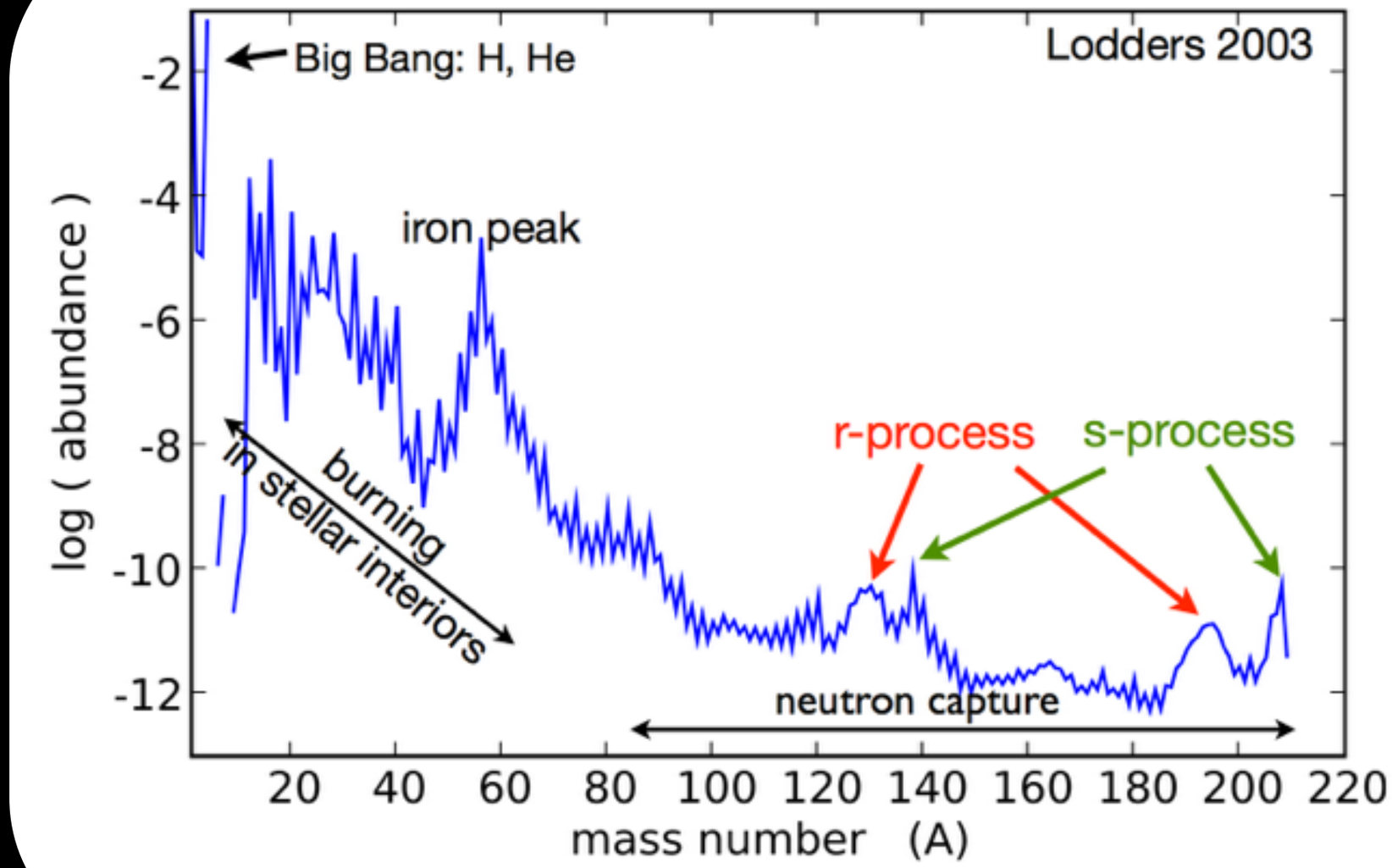
Lodders 2003
Big Bang: H, He
iron peak
burning
in stellar interiors
r-process
s-process
neutron capture
log (abundance)
-2
-4
-6
-8
-10
-12
20
40
60
80
100
120
140
160
180
200
220
mass number (A)

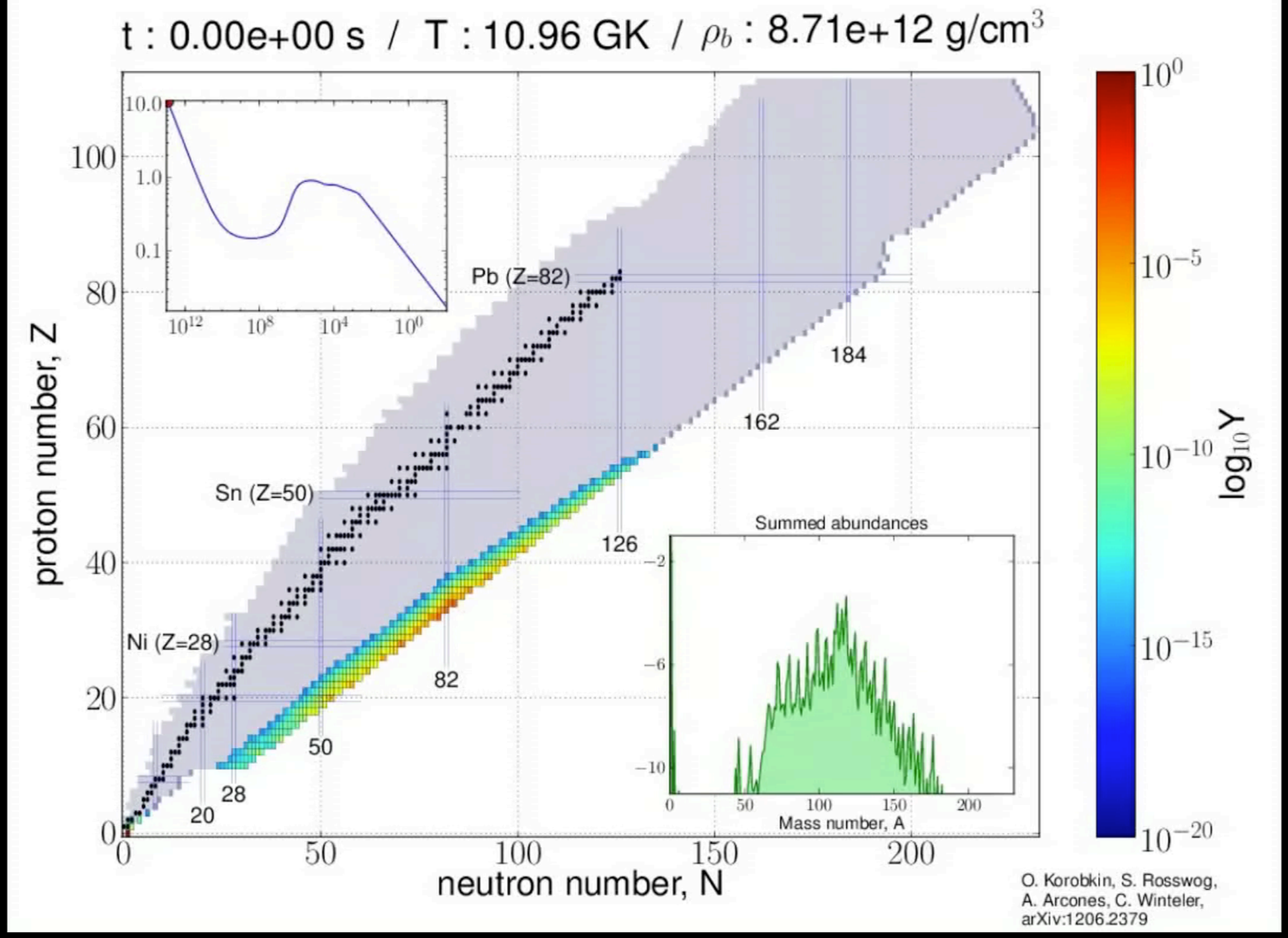
t : 0.00e+00 s / T : 10.96 GK / ρ_b : 8.71e+12 g/cm^3
proton number, Z
neutron number, N
Pb (Z=82)
Sn (Z=50)
Ni (Z=28)
20
28
50
82
126
162
184
Summed abundances
Mass number, A
$\log_{10}$ Y
O. Korobkin, S. Rosswog,
A. Arcones, C. Winteler,
arXiv:1206.2379

Heating Rates

$$\dot{Q}_r = M X_r \dot{\epsilon}_r$$

$$\dot{\epsilon}_r \simeq 2 \times 10^{10} \left(\frac{t}{1\,\mathrm{day}} \right)^{-1.3} \mathrm{erg/g/s}$$

Why a power-law instead of an exponential for radioactive decay?

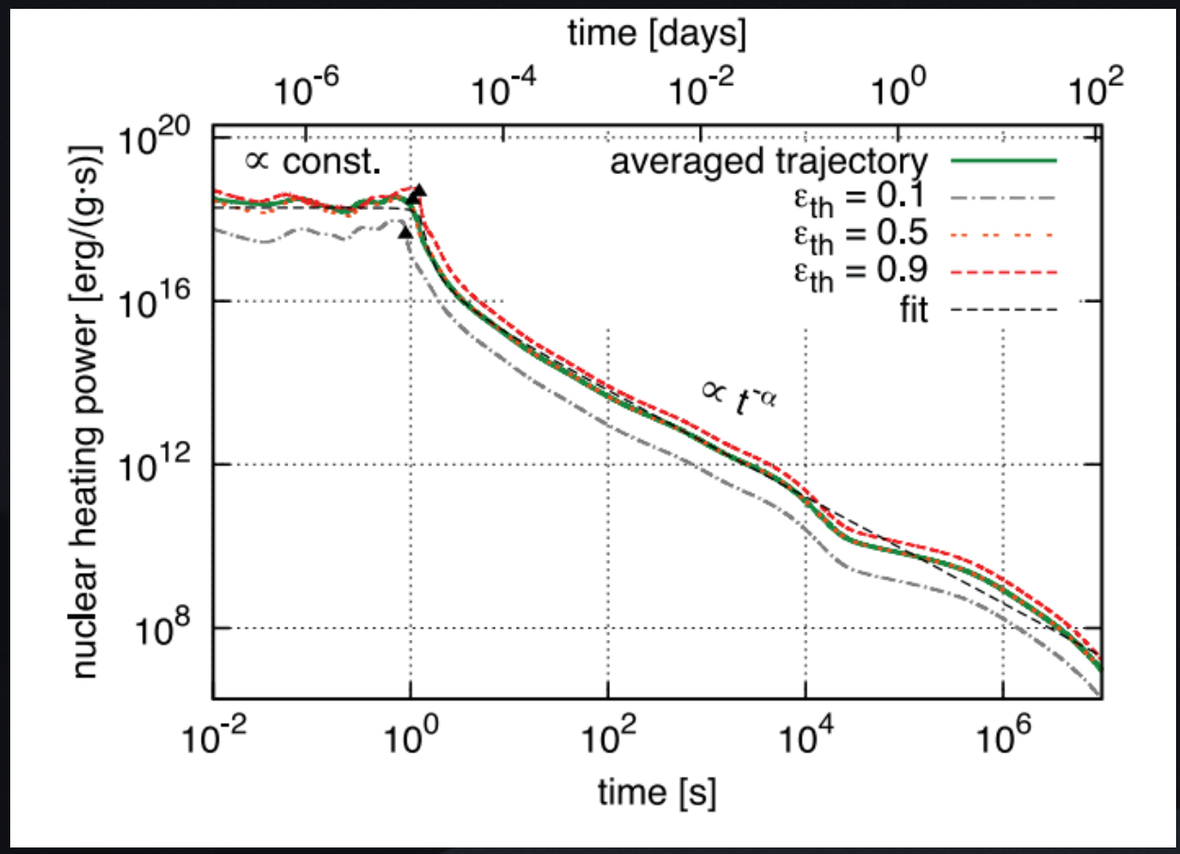

(Korobkin+2012)

The power-law is given by considering the overall decay of many species with different decay time

For the single species with decay time t_r we have that:

$$N_r(t) \propto e^{-t/t_r} \qquad \dot{N}_r(t) \propto \frac{e^{-t/t_r}}{t_r}$$

Let's assume that the characteristic heating rate time are equally distributed in log(t) in the interval $t_{min} < t_r < t_{max}$

$$\dot{N}(t) \simeq \frac{N}{\lambda_r} \int_{t_{min}}^{t_{max}} \frac{e^{-t/t_r}}{t_r} \frac{1}{t_r} dt_r$$

Normalisation factor

Rate of the elements with t_r

Distribution of decay with t_r

Solving by substituting $u = t/t_r$

$$\dot{N} \simeq \frac{N}{\lambda_r} \frac{e^{-t/t_{\max}}}{t}$$

$$\dot{n} = \frac{\dot{N}}{N\langle A\rangle m_p} \propto t^{-1}$$

The number of decays per unit time per gram scales as t^{-1}

However, for $\beta-$ decays, longer lived isotopes releases lower energy

$$E_{\beta,r} \propto t_r^{-a} \qquad E_\beta(t) \simeq E_{\beta,r} \qquad \dot{\epsilon}_\beta = \dot{n}(t)E_\beta(t) \propto t^{-(1+a)}$$

The temporal behaviour is steeper than t^{-1}

Non-relativistic (relativistic) Coloumb regime applies (Hotokezaka+2016), such that a = 1/3 (a = 1/4)

$$1 + a \sim 1.3$$

Thermalization Efficiency

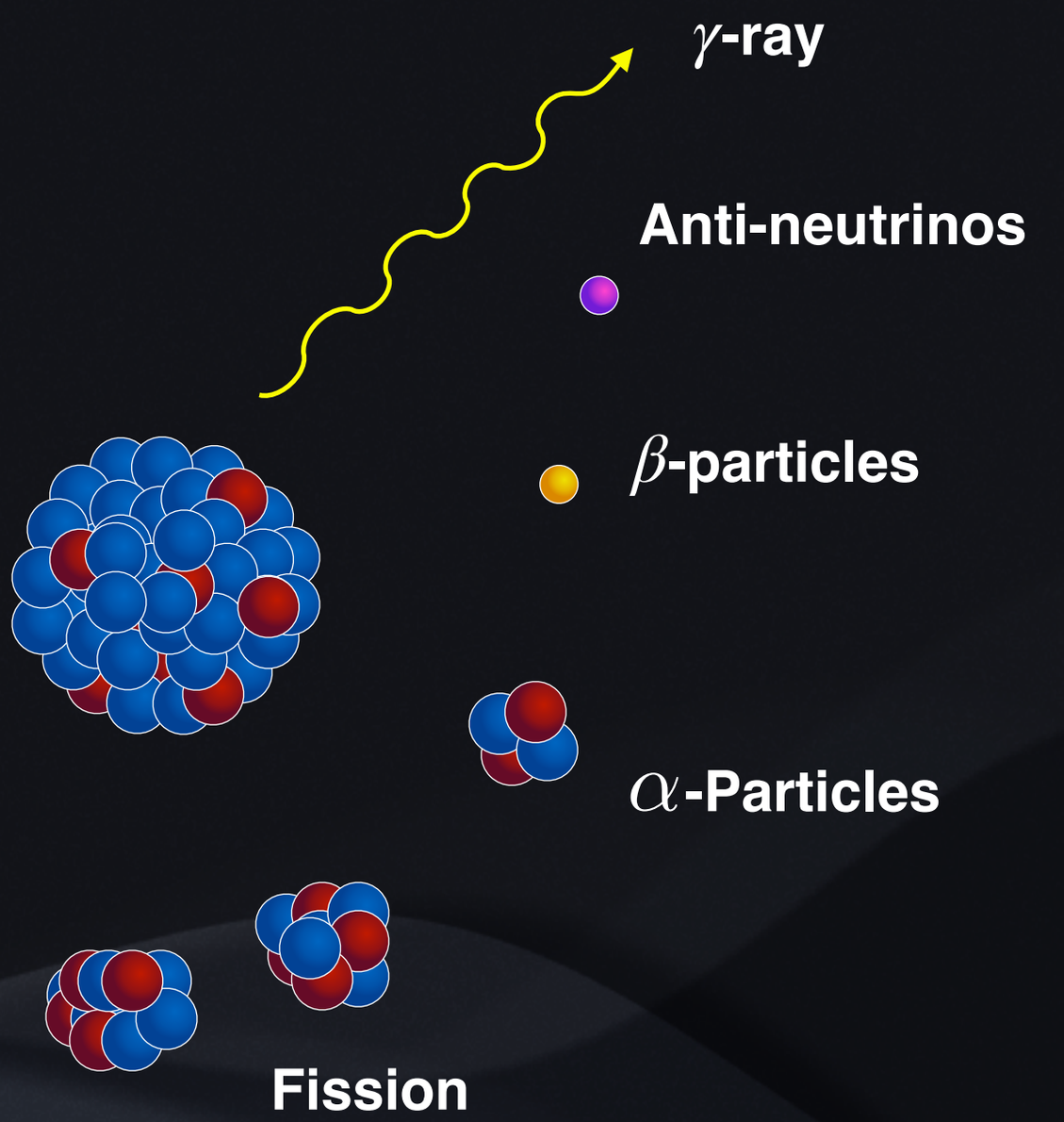

Energy released during the radioactive decay is in form of non-thermal particles.

They have to thermalize to share their energy with the ejecta

They can do it through different processes, with a time-dependant efficiency

Main reference: Barnes+2016

Thermalization Efficiency

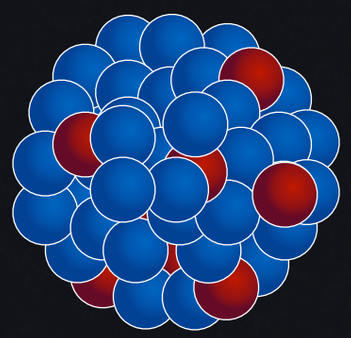

Fission Fragments

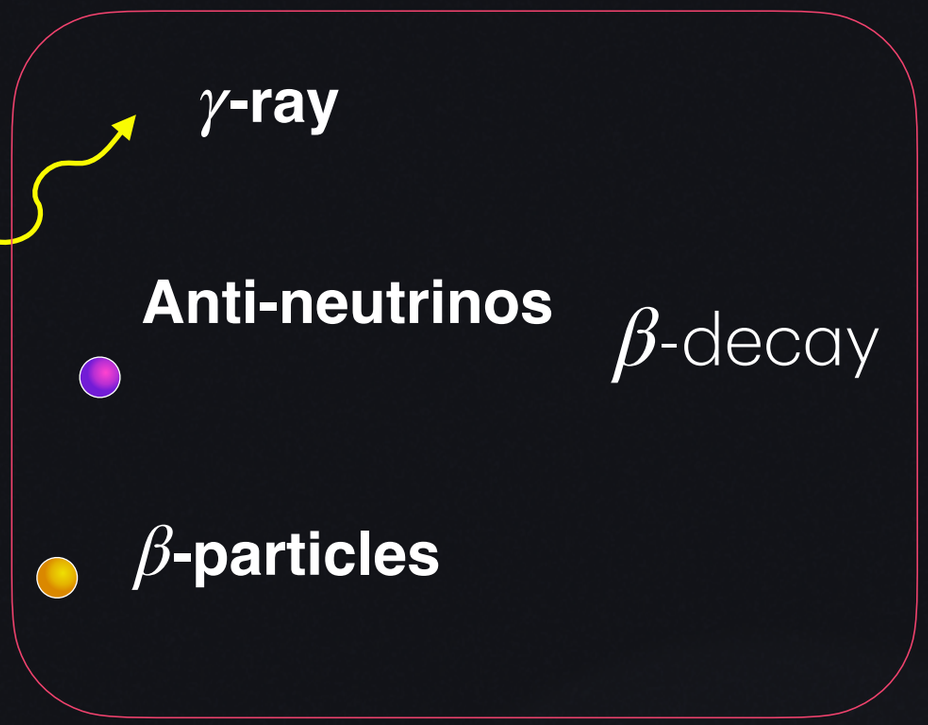

α-Particles

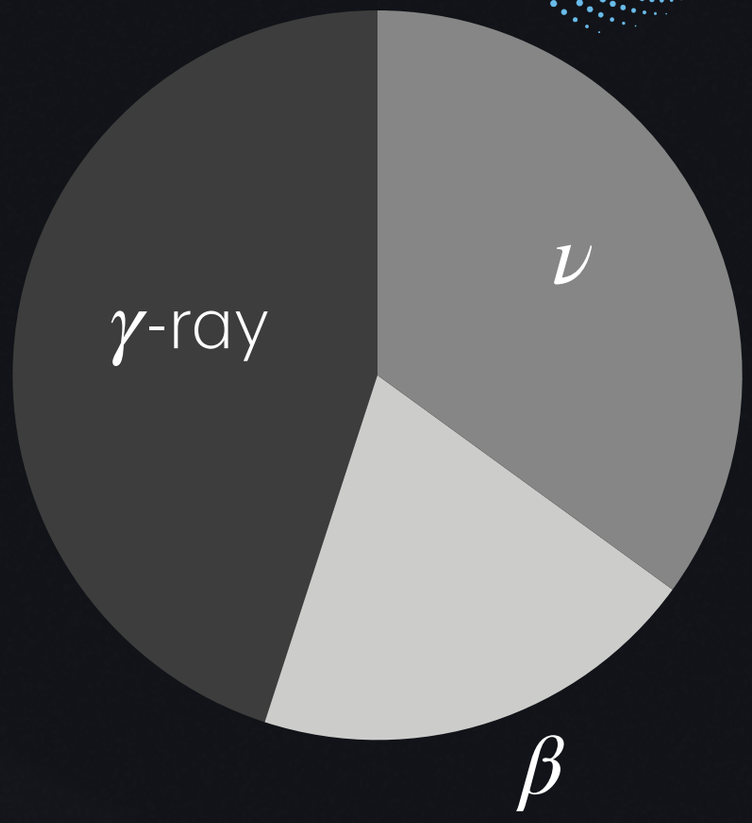

For example, in β-decay, 20% of the energy goes in electrons, 45% in γ-rays, and 35% in neutrinos (Barnes +2016).

Neutrinos do not thermalise. Only max ~65% of β-decay energy available for thermalisation

Main reference: Barnes+2016

Thermalization Efficiency

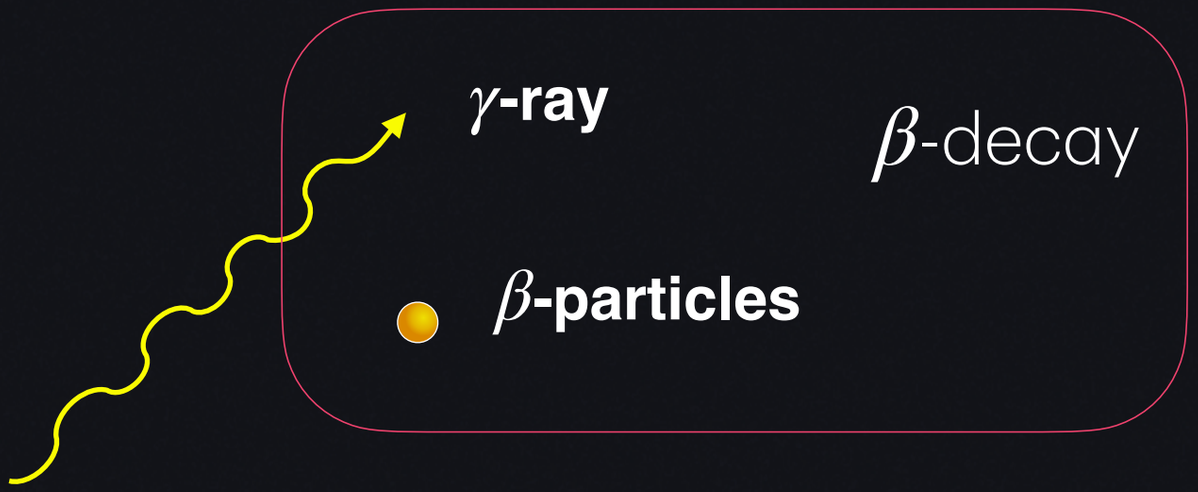

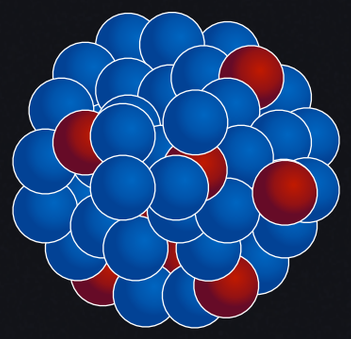

γ-rays thermalise through **photoionization** ($\lesssim 1\,MeV$) and through **Compton scattering ($\gtrsim 1\,MeV$)**

β particle thermalise through **plasma losses** (Coulomb interactions with free thermal electrons), **excitation and ionisation of bound electrons** and **Bremsstrahlung** (at VHE)

Thermalization Efficiency

α-particles thermalize by interacting with free and bound electrons.

Fission fragments thermalize by interacting with free and bound electrons and atomic nuclei

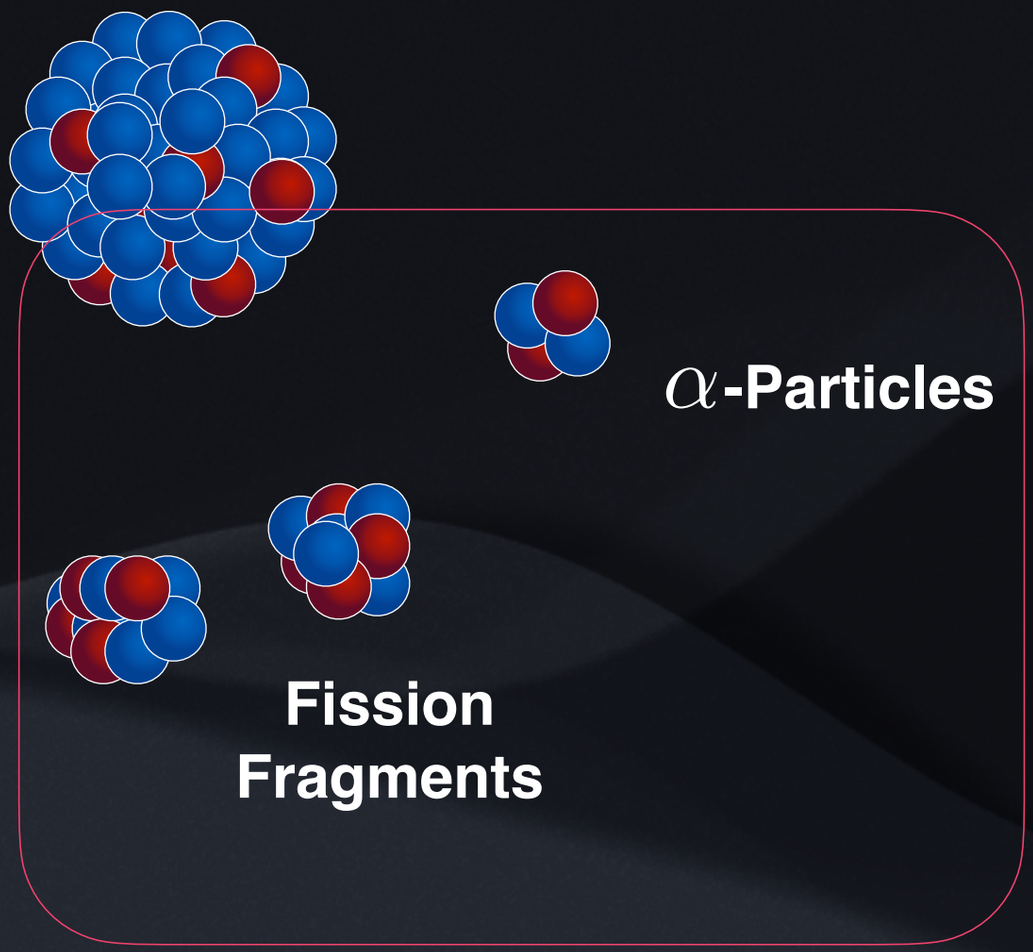

However, α-decay occurs mainly in translead nuclei (Z>82) and fission fragments for heavier nuclei. Their synthesis depends on the electron fraction

Thermalization Efficiency

Thermalization efficiency depends on density, so on M_{ej} and v and and time. It decreases in time. It is maximum for fission fragments > $\alpha > \beta > \gamma$

Thermalization becomes inefficient **after the peak** for most β, for α and fission fragments. It is inefficient **before the peak** for γ

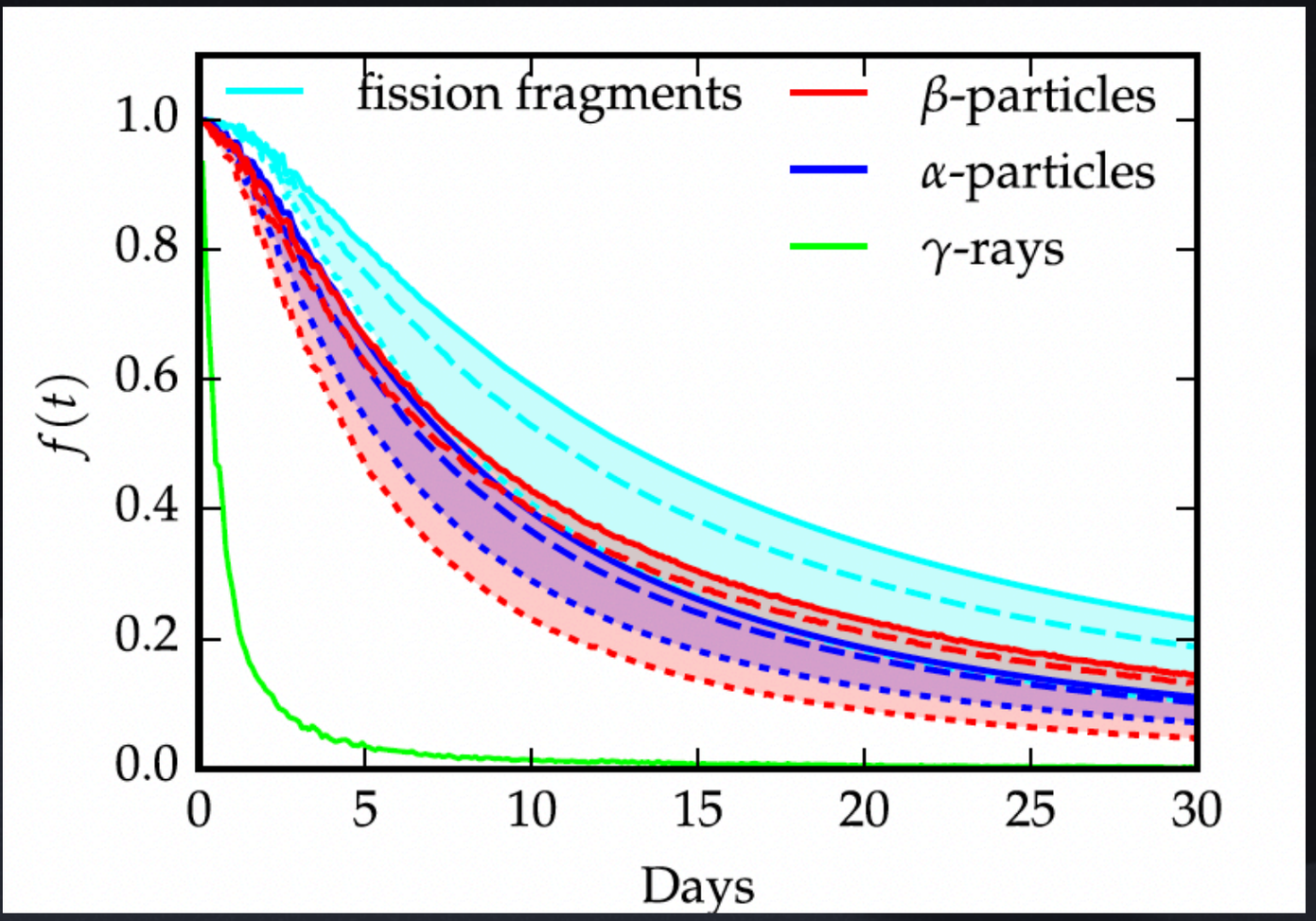

(Barnes + 2016)

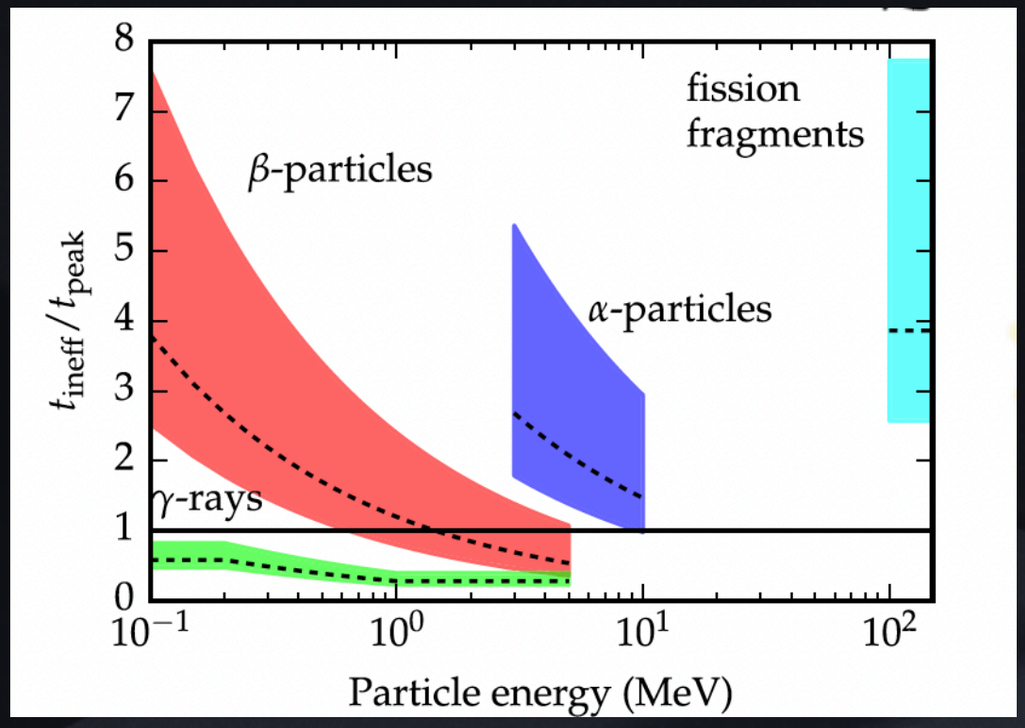

(Barnes + 2016)

Opacity

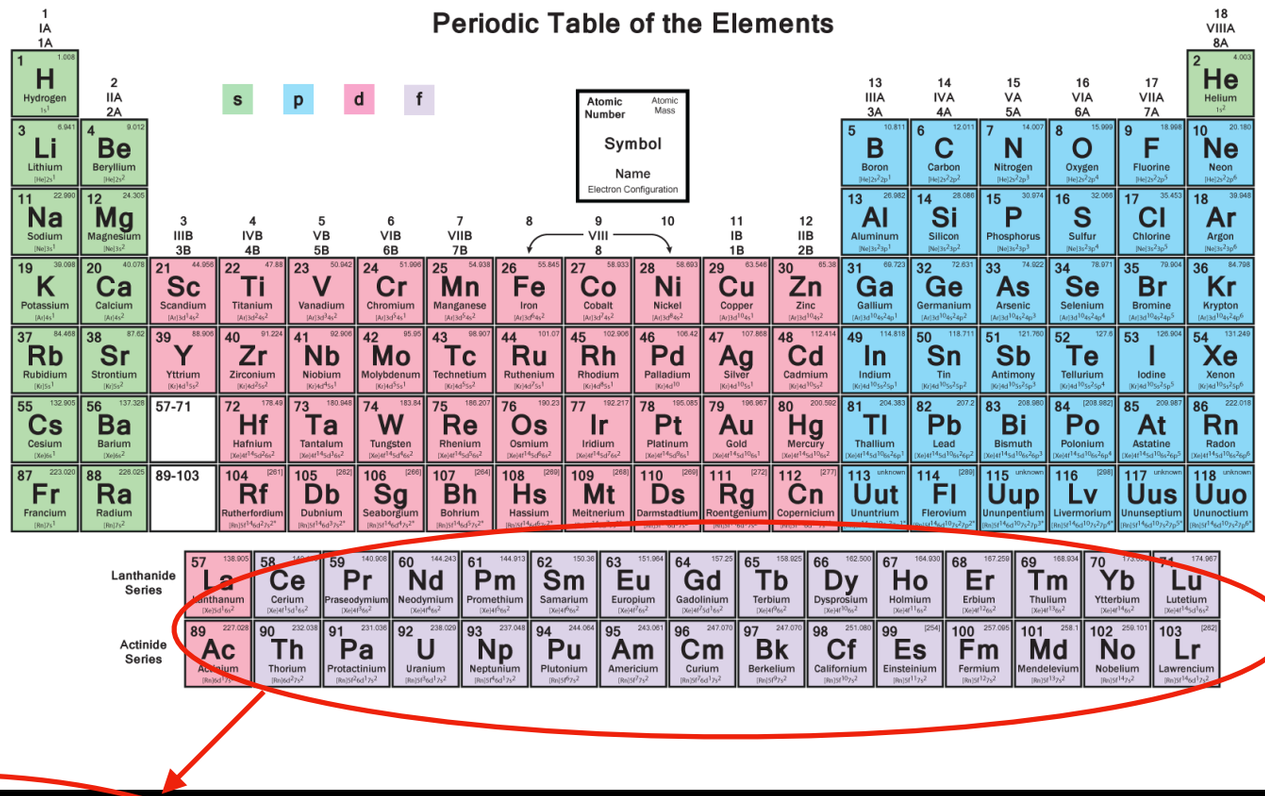

Lanthanides & Actinides:

Open electron valence f-shell

Complex electronic structure

High number of transitions

High Opacity

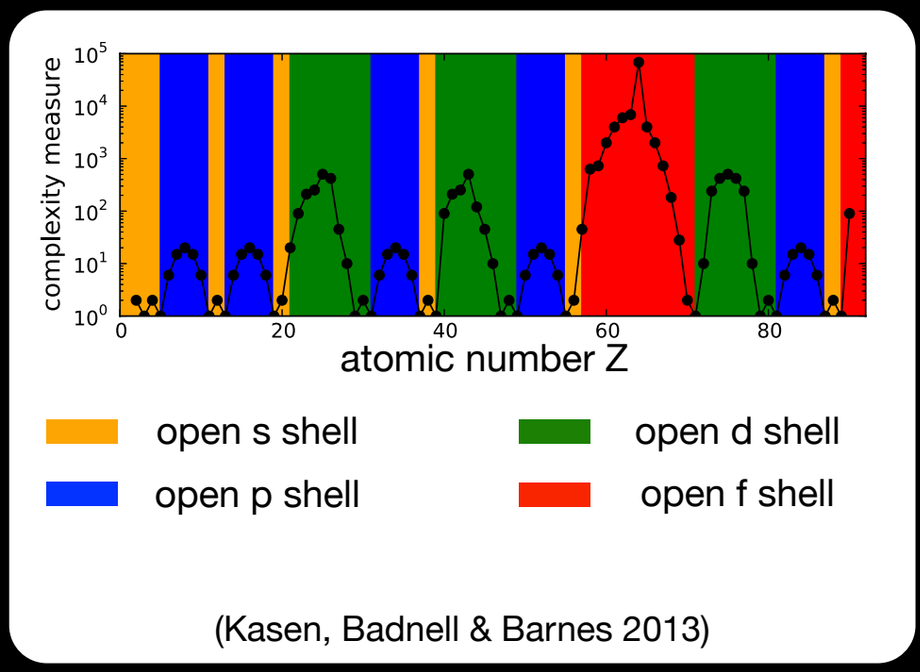

(Kasen, Badnell & Barnes 2013)

Opacity

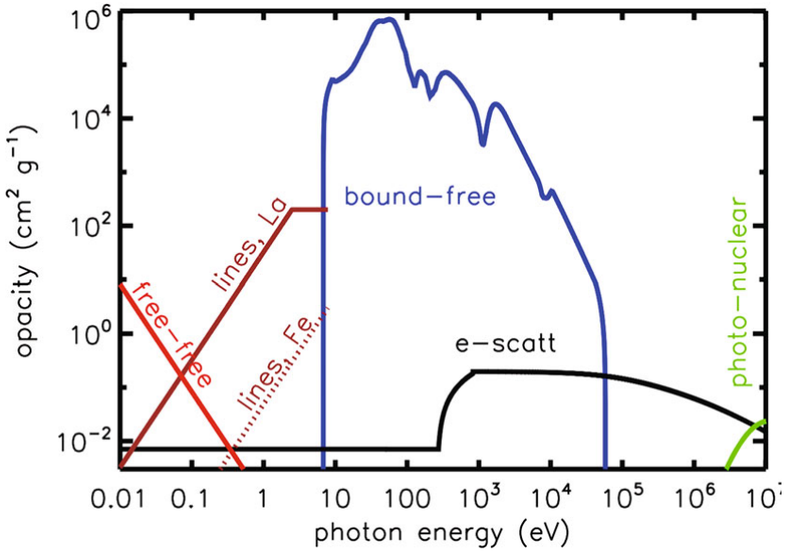

(Metzger 2020)

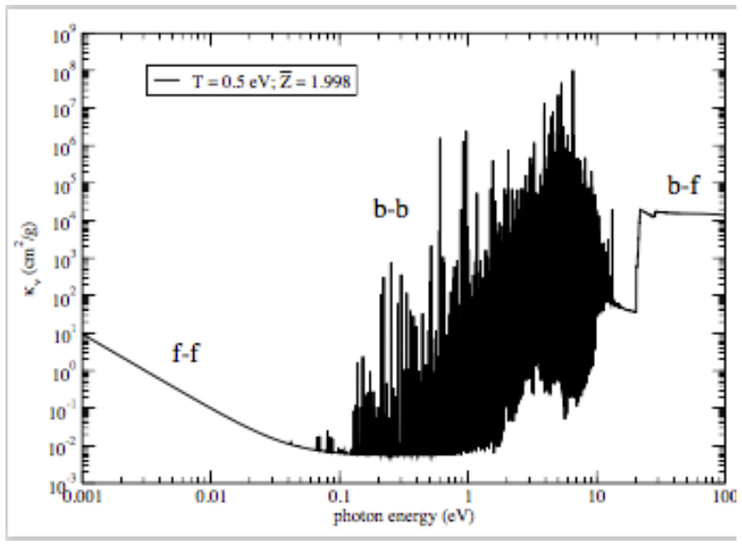

(Fontes et al. 2017)

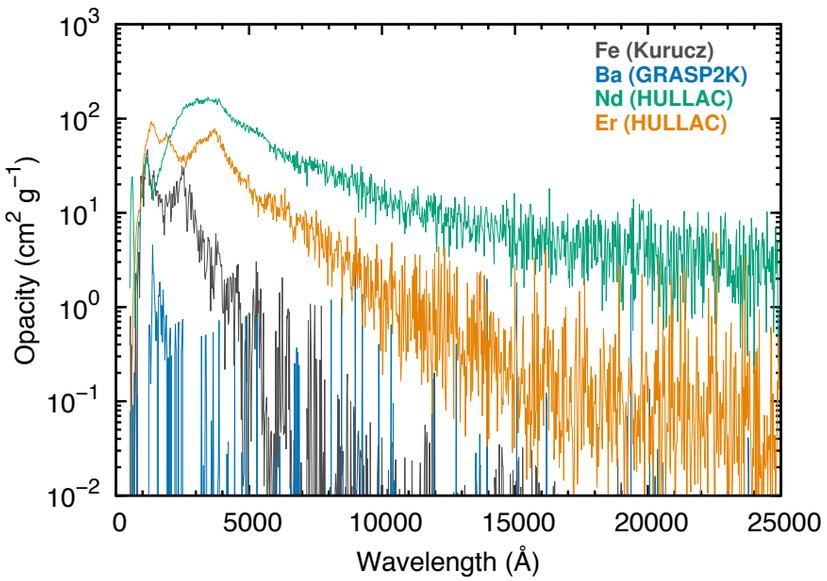

(Tanaka et al. 2017)

Radio - Far IR → Free - Free absorption

Near IR - Optical → Bound - Bound transitions

UV - X-ray → Bound - Free transitions

X-ray - γ-ray → Electron scattering

Nucleosynthesis and Opacity

$Y_e < 0.2$, r-process up to the 3rd peak $\mathrm{A} \sim 195$ (lanthanide rich) → $k < 20 - 30\,\mathrm{cm}^2/\mathrm{g}$

$0.25 < Y_e < 0.35$, r-processes up to the 2rd peak $\mathrm{A} \sim 130$ (few or no lanthanides) → $k \sim 3 - 5\,\mathrm{cm}^2/\mathrm{g}$

$Y_e \sim 0.40$, Fe group elements, with few or none r-process elements → $k \sim 1\,\mathrm{cm}^2/\mathrm{g}$

Tanaka+2020

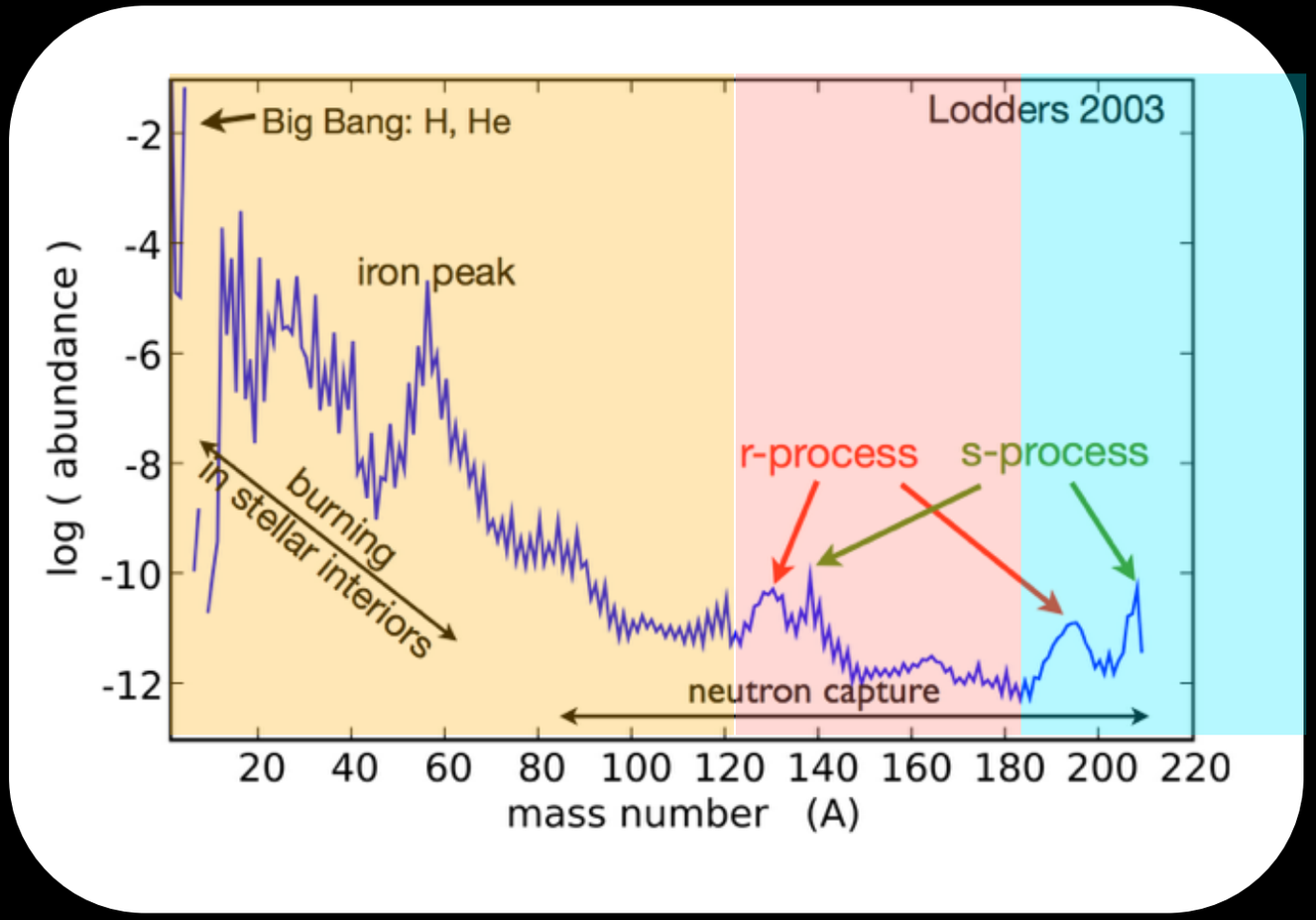

Thermodynamic Equilibrium

Local Thermodynamic Equilibrium

- Ionization and excitation state of matter impact the opacity
- But how we calculate them?
- In LTE we assume that collision processes dominates the excitation and ionization rates.

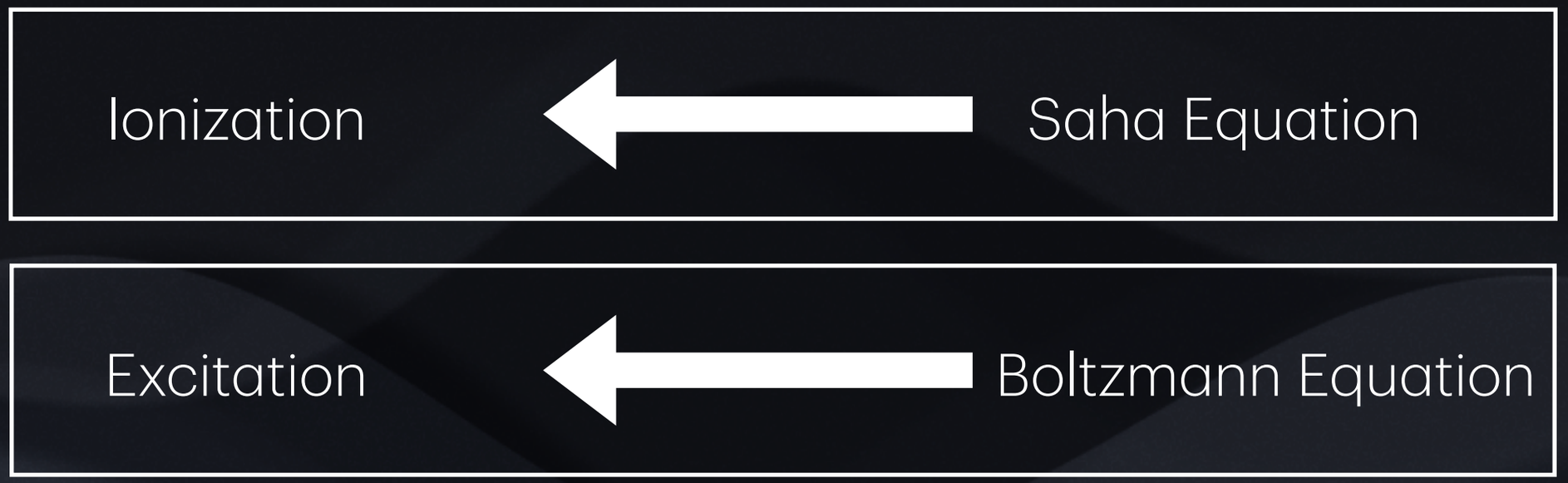

- Local temperature determines the ionization and excitation state of atoms

Thermodynamic Equilibrium

Local Thermodynamic Equilibrium

- LTE valid when collision dominates and/or radiation field is thermal, i.e. at high density and/or optically thick medium

- But what happens when the density drops and the KN enters its nebular phase?

- LTE no longer a good approximation

Thermodynamic Equilibrium

Local Thermodynamic Equilibrium

- LTE valid when collision dominates and/or radiation field is thermal, i.e. at high density and/or optically thick medium

- But what happens when the density drops and the KN enters its nebular phase?

- LTE no longer a good approximation

Thermodynamic Equilibrium

Non-Local Thermodynamic Equilibrium

- The ionization and excitation state depends on the radiation field

- ...which also depends on the ionization and excitation state

Thermodynamic Equilibrium

Non-Local Thermodynamic Equilibrium

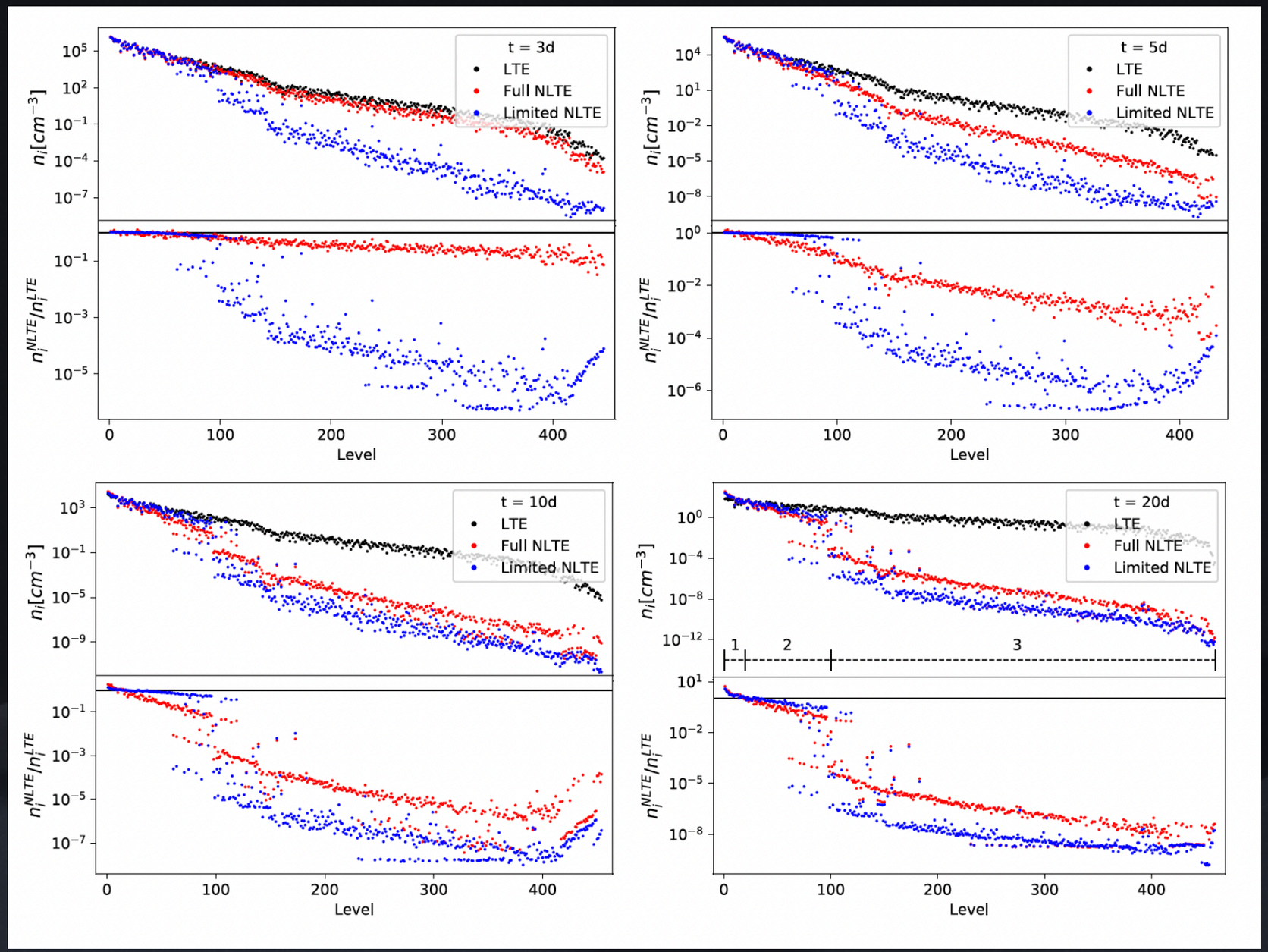

Level population of Ce II (Pognan+2022)

Thermodynamic Equilibrium

Non-Local Thermodynamic Equilibrium

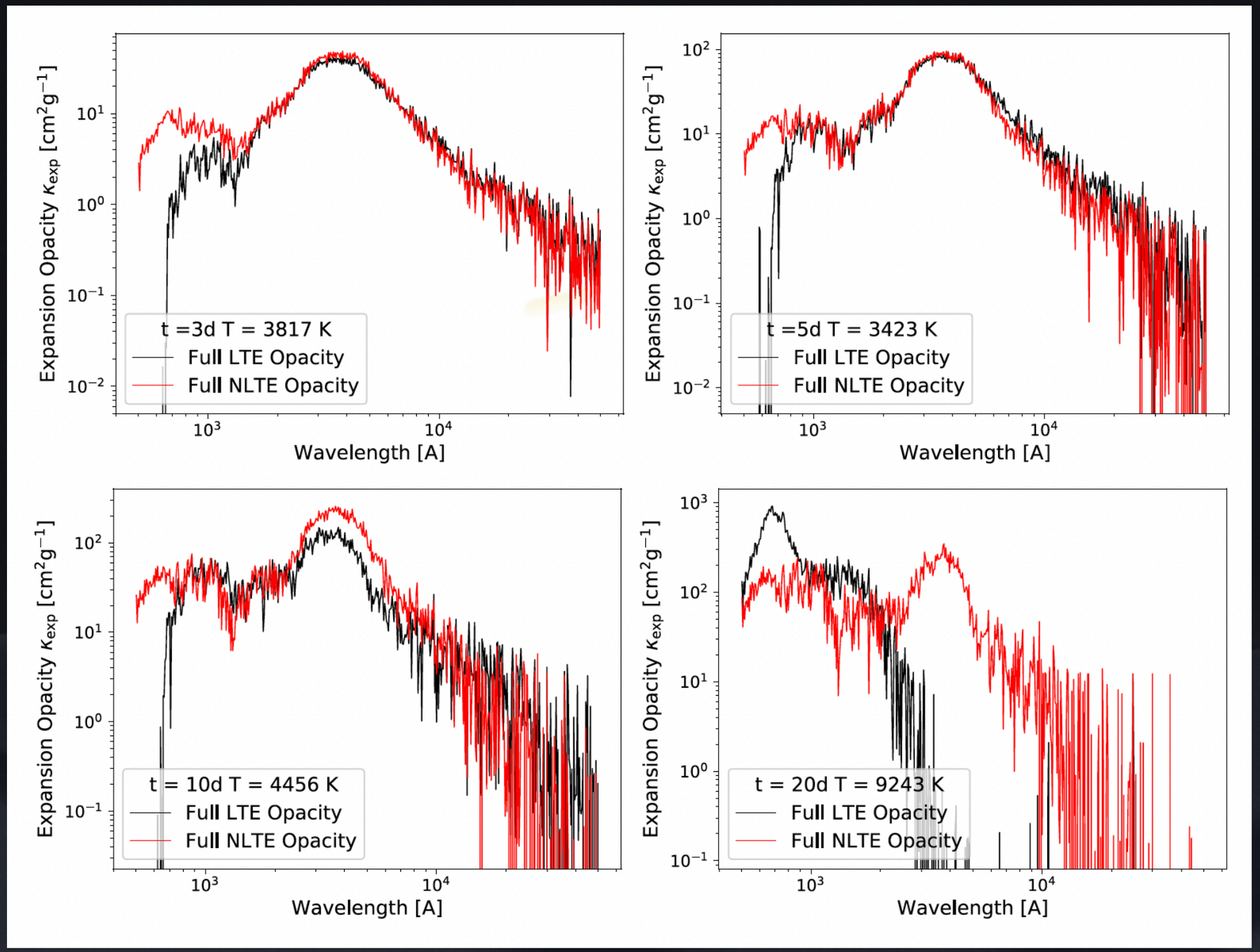

Expansion opacities LTE vs NLTE (Pognan+2022)

Multiple ejection channels

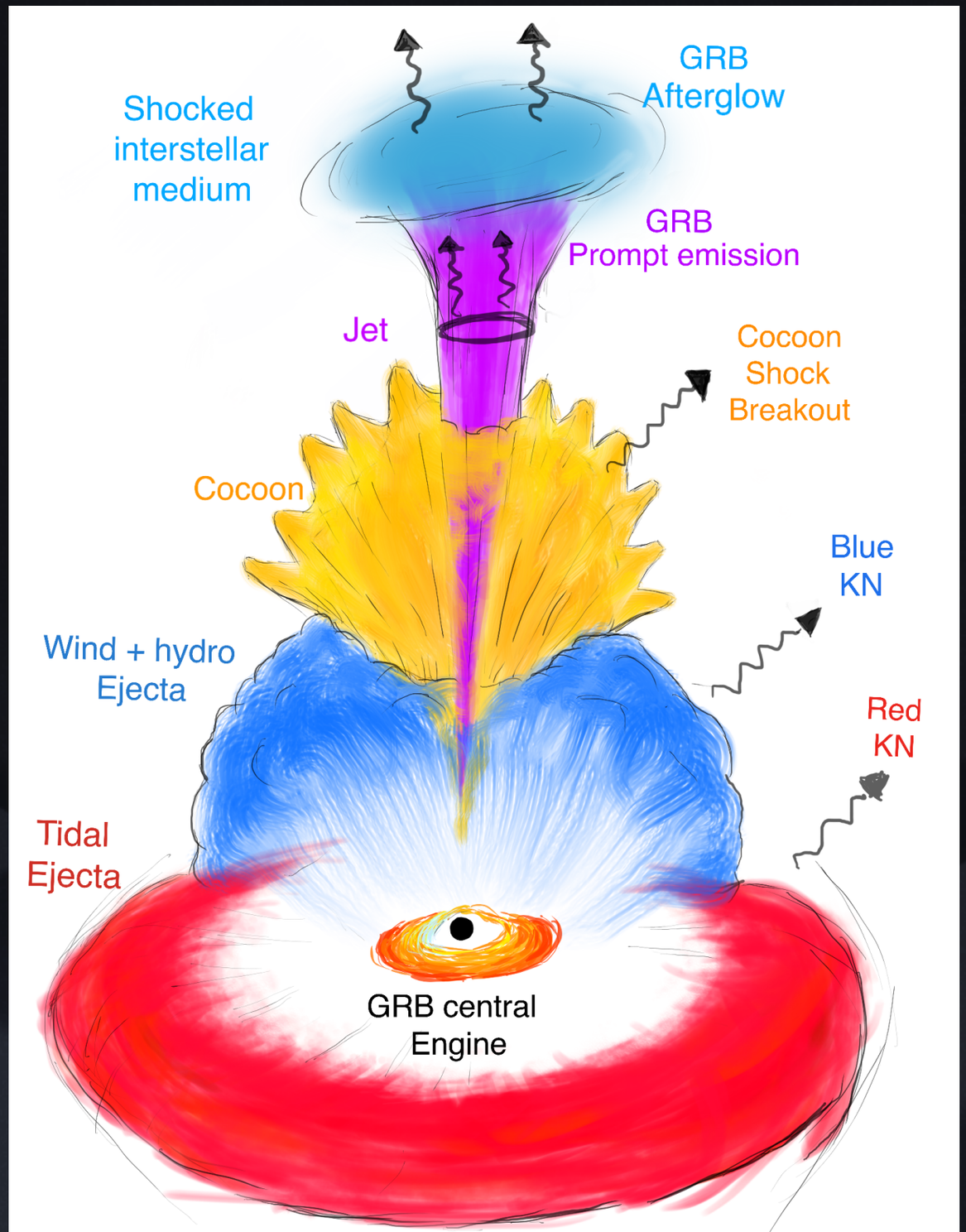

Ascenzi et al. 2021

ACME
Astrophysics Centre for Multimessenger studies in Europe

Shocked Dynamical Ejecta (Only for BNS)

Wind Ejecta

Viscous (secular) Ejecta

Tidal Dynamical Ejecta

Dynamical Ejecta

$t \sim \mathcal{O}(ms)$ $\quad v_{\rm dyn} \sim 0.2 - 0.3\,c$

$M_{\rm dyn}^{\rm BNS} \sim 10^{-4} - 10^{-3}\,M_\odot$ → Depends on mass ratio, total mass and EOS

$M_{\rm dyn}^{\rm NS-BH} \sim 0 - 10^{-1}\,M_\odot$ → Depends on mass ratio, EOS, BH mass and spin

Tidal Ejecta →
- Both in BNS and NS-BH
- Along the equatorial plane
- Cold matter (low Y_e)
- Asymmetric binaries expelling more mass

Shocked Ejecta →
- Only in BNS
- Ejected by the quasi-radial pulsation of the remnant
- All the directions
- Hot matter (high Y_e)

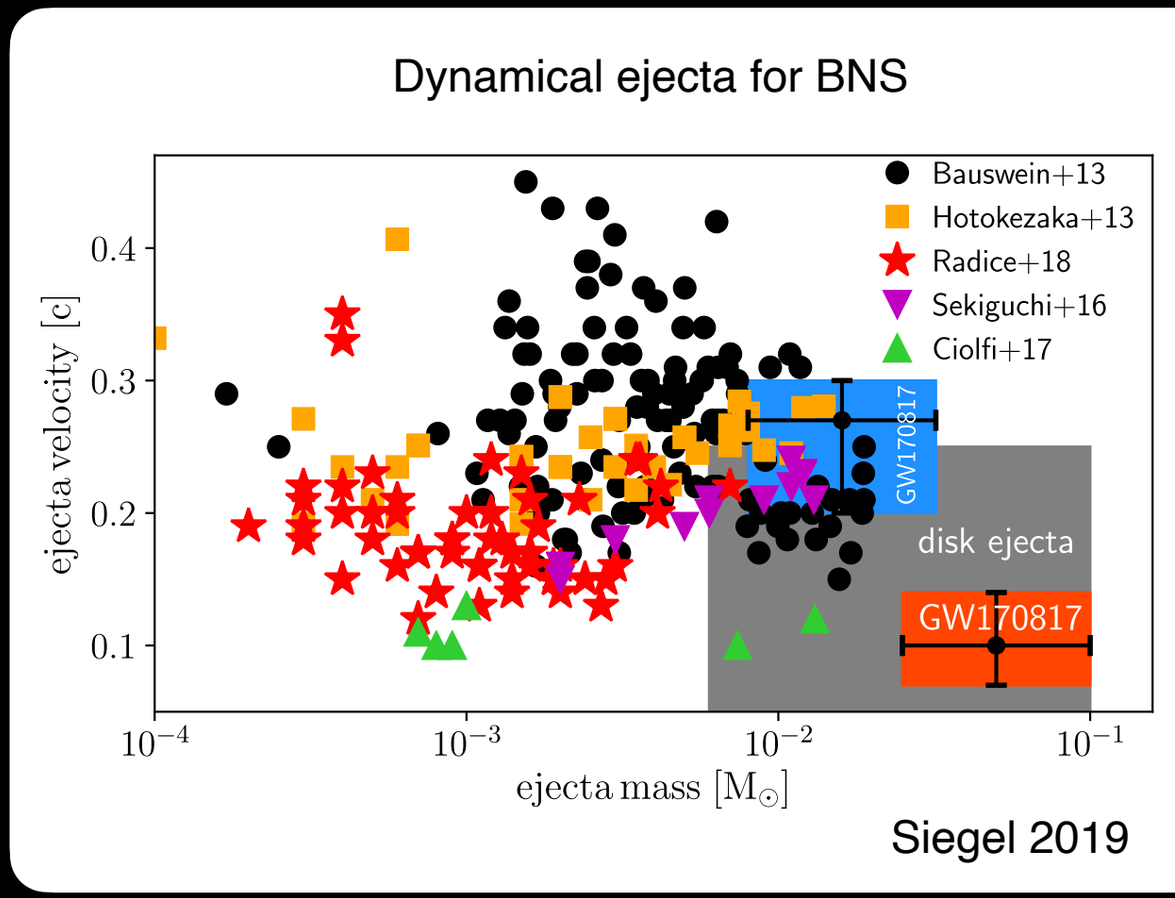

Siegel 2019

Wind Ejecta from the disk

- Both the metastable NS and the accretion disk emits neutrinos with a luminosity of $L_\nu \sim 10^{53}\,\mathrm{erg/s}$
- A fraction of neutrinos are absorbed and deposit their energy in the disk
- When the deposited energy overcomes the gravitational binding energy an outflow with $\dot{M} \sim 10^{-3}\,M_\odot/s$ and $v < 0.1\,c$ is generated, this happens on a timescale of $t_{wind} \sim 10\,\mathrm{ms}$
- **5%** of disk mass unbind
- If the metastable NS survives for more than 50 ms, $\sim 10^{-3}\,M_\odot$ can be also unbound from the NS surface . This can be substantially increased if the star has a strong ordered magnetic field (Metzger+2018).
- The lifetime of the metastable NS influences the Y_e of the ejecta

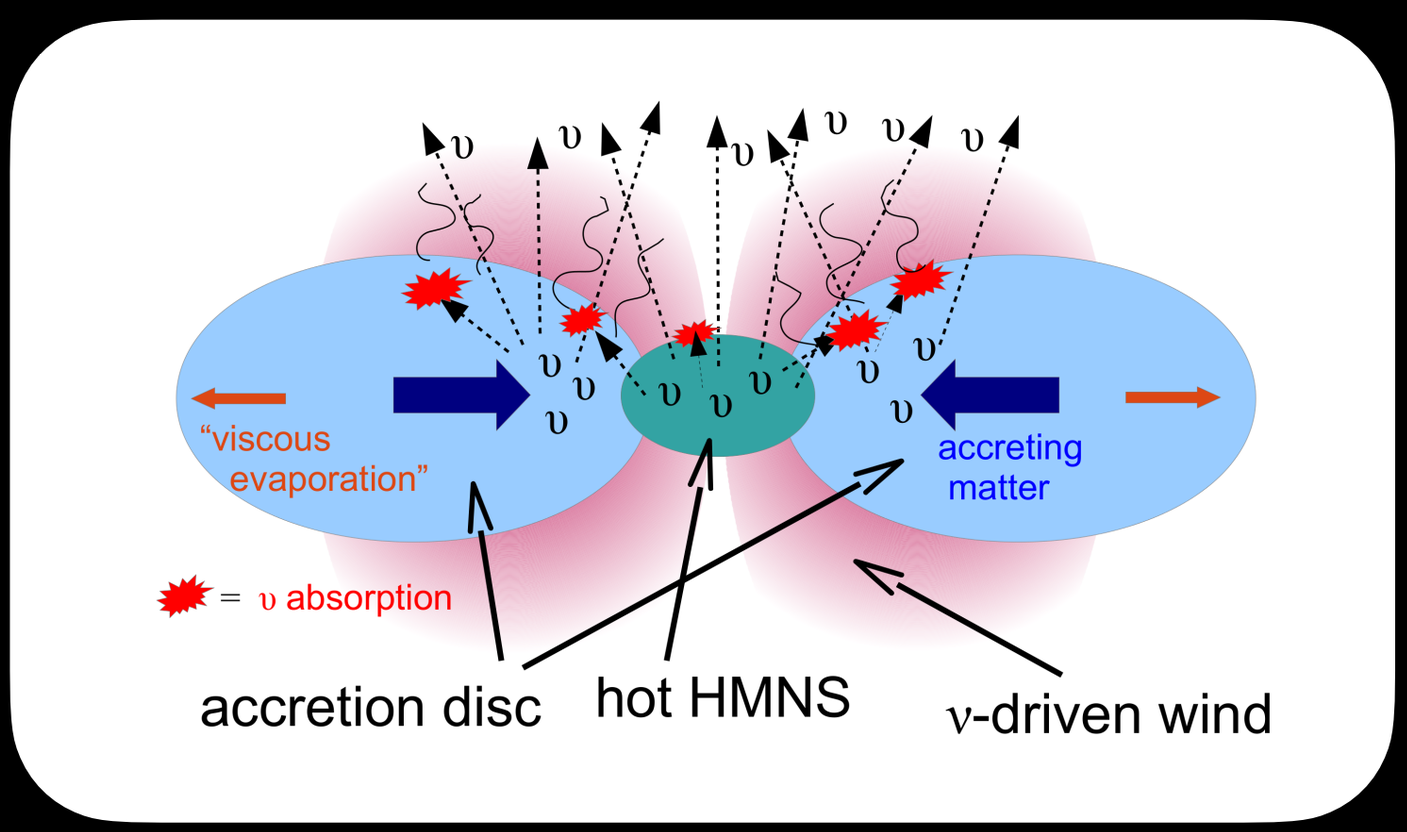

Perego+2014

Viscous secular ejecta

- When the accretion rate decreases the neutrino cooling is quenched. The heating due to viscosity and nuclear recombination are not balanced anymore by the neutrino cooling and an outflow is launched.
- The disk settles in a mildly degenerate state, where the pair production is suppressed (Beloborodov 2003, Siegel & Metzger 2017). The number density of electrons overcomes that of positrons. Electron capture by protons favoured with respect to positron capture by neutrons. **The outflow is neutron rich**, with $0.1 < Y_e < 0.4$.

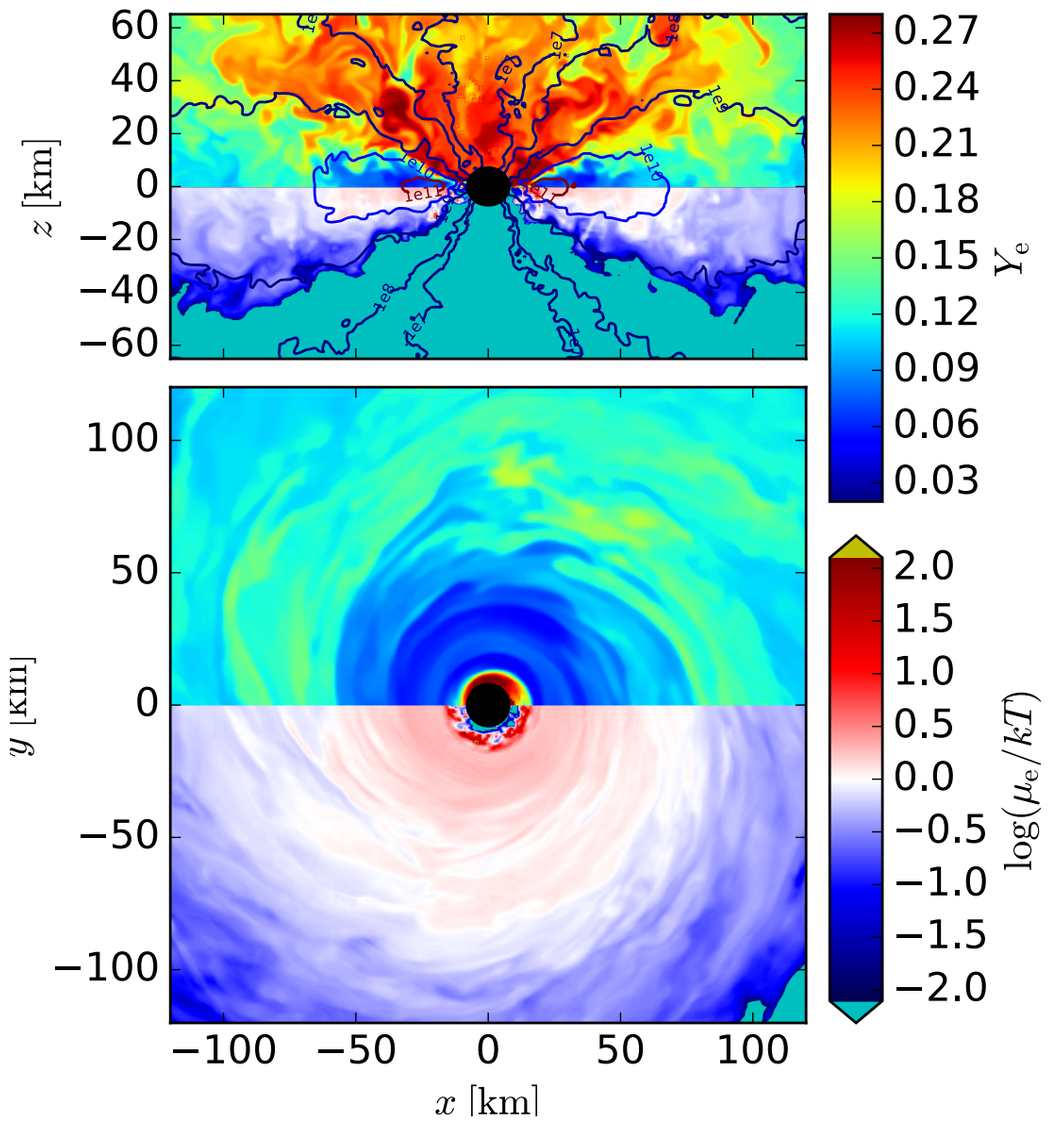

Siegel & Metzger 2017

$p + e^- \rightarrow n + \nu_e$ Favoured

$n + e^+ \rightarrow p + \bar{\nu}_e$ Disfavoured

- Up to 40% of disk mass unbound
- A long lived NS can generate an increase of Y_e

Dynamical Ejecta vs Disk Outflow

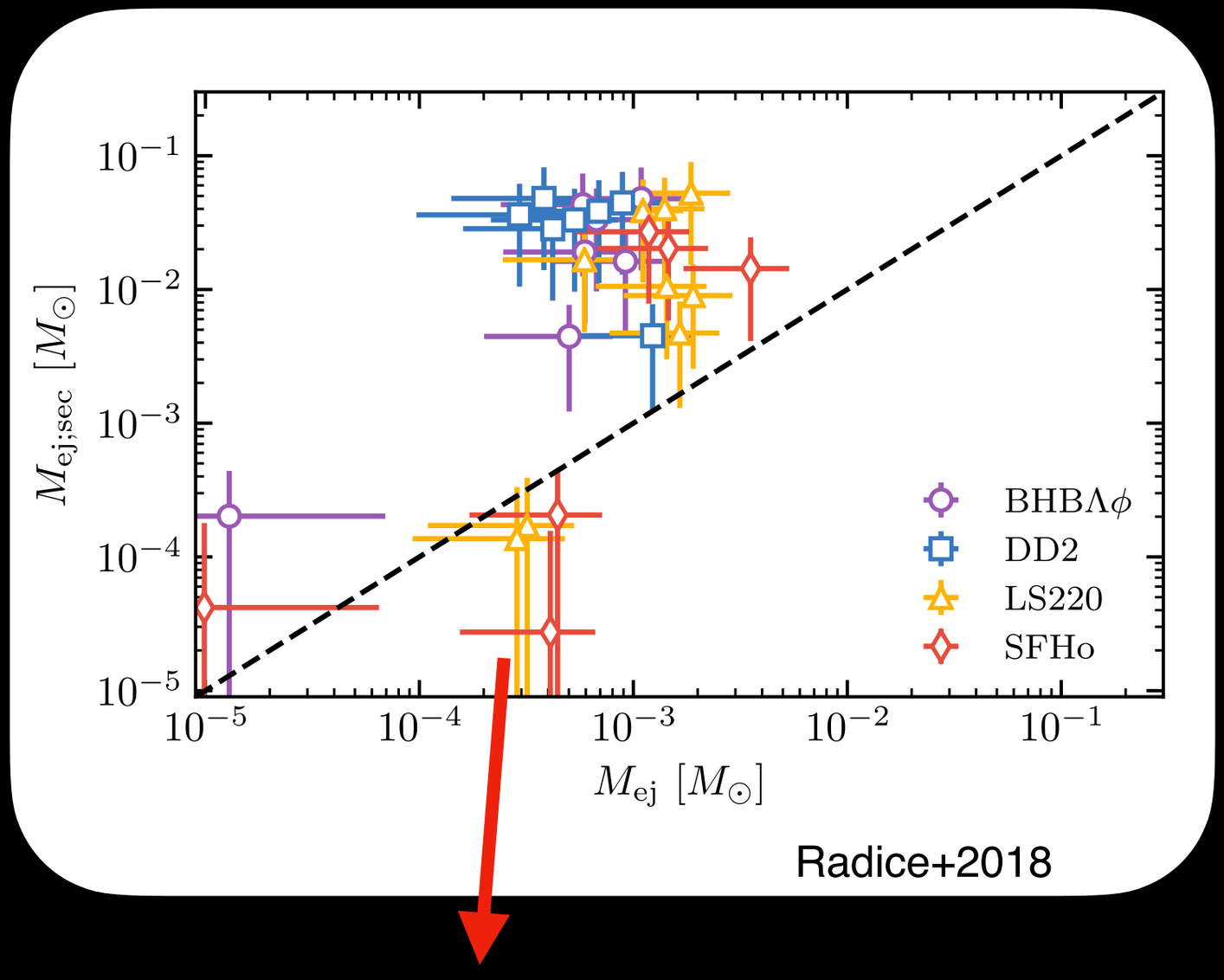

Radice+2018

Viscous Ejecta dominates over the dynamical ejecta in therms of mass content

Prompt BH formation

Kilonova Models

- Full Monte Carlo radiative transfer: e.g. SEDONA (Kasen 2006, Kasen+ 2017), ARTIS (Kromer & Sim 2009), Tanaka & Hotokezaka code (Tanaka & Hotokezaka 2013), SuperNu (Wollaeger+2013)
- Monte Carlo radiative transfer with simplified microphysics: e.g. POSSIS (Bulla 2019)
- Diffusion, grey opacity (e.g. Ricigliano+2024)
- Energy Balance (e.g. Metzger+2020)

Full Monte-Carlo Radiative Transfer

The Main Idea

$$\frac{dI_\nu}{ds} = j_\nu - \alpha_\nu I_\nu$$

Radiative transfer equation

I_ν : Specific intensity

j_ν : Emission coefficient

$\alpha_\nu = \rho k_\nu$: Absorption coefficient

Full Monte-Carlo Radiative Transfer

The Main Idea

$$\frac{dI_\nu}{d\tau_\nu} = S_\nu - I_\nu$$

Radiative transfer equation

$d\tau_\nu = \alpha_\nu ds$, τ_ν : optical depth

$S_\nu \equiv \frac{J_\nu}{\alpha_\nu}$: Source Function

$$I_\nu(\tau_\nu) = I_\nu(0)e^{-\tau_\nu} + \int_0^{\tau_\nu} e^{-(\tau_\nu - \tau'_\nu)} S_\nu(\tau'_\nu) d\tau'_\nu$$

Formal solution

Full Monte-Carlo Radiative Transfer

The Main Idea

$$\frac{dI_\nu}{d\tau_\nu} = S_\nu - I_\nu$$

Radiative transfer equation

The idea of Monte Carlo radiative transfer is to describe transport as a sequence of stochastic events representing the interaction of radiation with the medium.

Photon packets with sampled frequency, direction and (optionally) polarization are injected into the ejecta and evolved in time.

Each packet propagates over a distance set by a random optical depth and then undergoes an interaction (e.g. absorption, scattering) drawn from probabilities governed by the local microphysics (e.g. opacities and emissivities).

Packets that escape the computational domain are recorded, and the emergent radiation field (light curves and spectra) is reconstructed from their properties.

Full Monte-Carlo Radiative Transfer

The walkthrough of a particle...

Emission: a packet is created in a cell according to the local energy source. Its λ is sampled from the local emissivity and its direction drawn isotropically in the comoving frame

Propagation: the packet is propagated through the expanding ejecta. Its comoving λ is redshifted because of homologous expansion

Event selection: the distance to the next possible event is computed: a continuum/line interaction, a cell boundary or time boundary reached. The smallest of this distance determines what happens.

Full Monte-Carlo Radiative Transfer

The walkthrough of a particle...

Interaction

Continuum event

The particle may be absorbed or scattered with probability set by local opacity.

Absorption

Re-emitted with a new λ sampled by the local emissivity

Scattering

comoving λ unchanged, new direction and polarisation

Line resonance

It interacts with probability set by the line optical depth.

It can be, absorbed and re-emitted (resonant), de-excited into a different transition (fluorescence)

Full Monte-Carlo Radiative Transfer

The walkthrough of a particle...

Escape

The sequence is repeated until the packet reaches the outer boundary of the ejecta

Escaping packets are binned by time, λ, direction and polarisation and the emergent radiation field is reconstructed from the full ensemble

Full Monte-Carlo Radiative Transfer

Microphysics, the example of SEDONA (Kasen 2006, Kasen+2017)

Radiation source & heating: analythc fits to $\dot{\epsilon}(t)$ and $\dot{\epsilon}_{th}(t, M_{ej}, v_{ej})$, MC γ-ray transport

Thermal state: local T obtain by rad. equilibrium: heating and photon absorption balanced by thermal emission.

Excitation & Ionization: computed in LTE

Lines: some lines ($< 5 \times 10^5$, Kasen 2006) can be treated one-by-one from Fe-group and lanthanides with multiple ionization, fluorescence included.

Continuum: by e-scattering, bound-free, free-free. Bound-bound ($\mathcal{O}(10^7)$ lines) described by expansion opacity formalism

...simplifying the microphysics

The example of POSSIS (Bulla 2019)

3D MC radiative transfer with viewing-angle dependence and polarisation.

Opacities are provided as input, not computed self-consistently.

Heating, thermalisation, density and temperature evolution from analytic prescriptions

In Bulla 2023 expansion opacity from Tanaka+2020 (see previous slides) as input

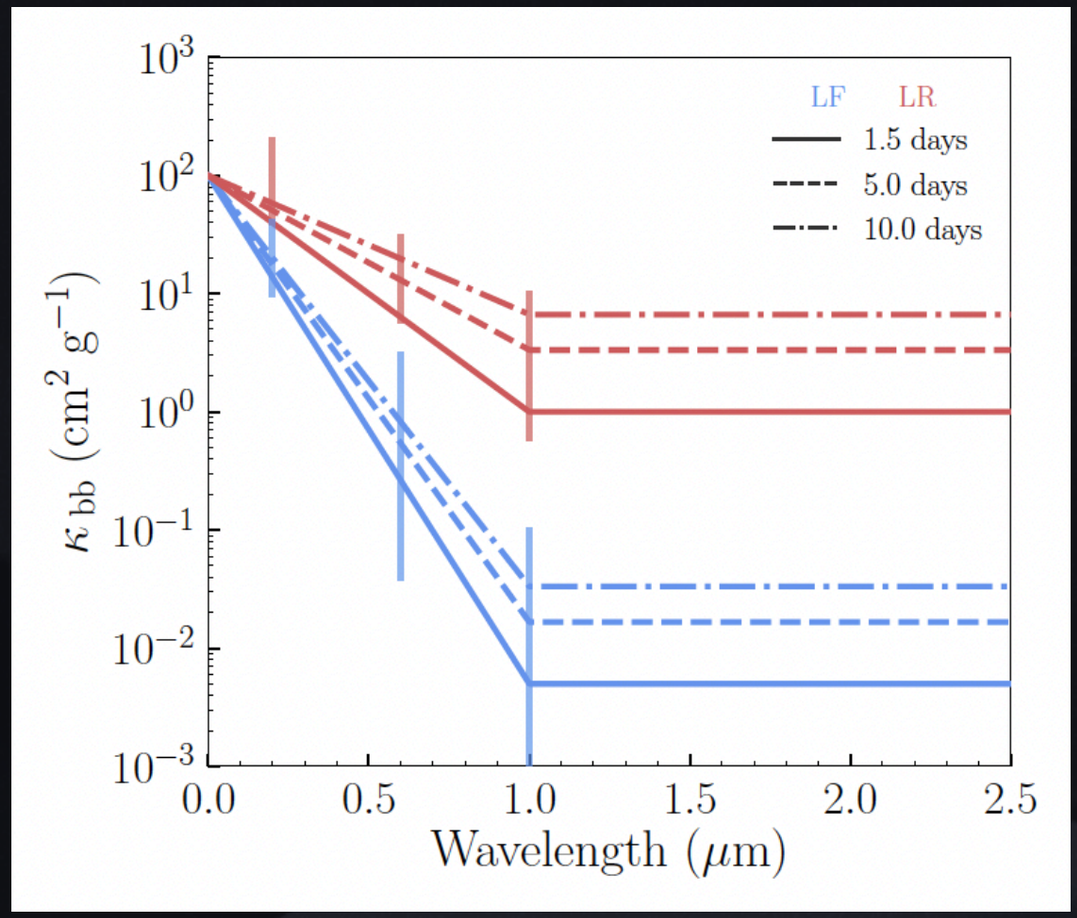

(Bulla 2019)

...simplifying the microphysics

The example of POSSIS (Bulla 2019)

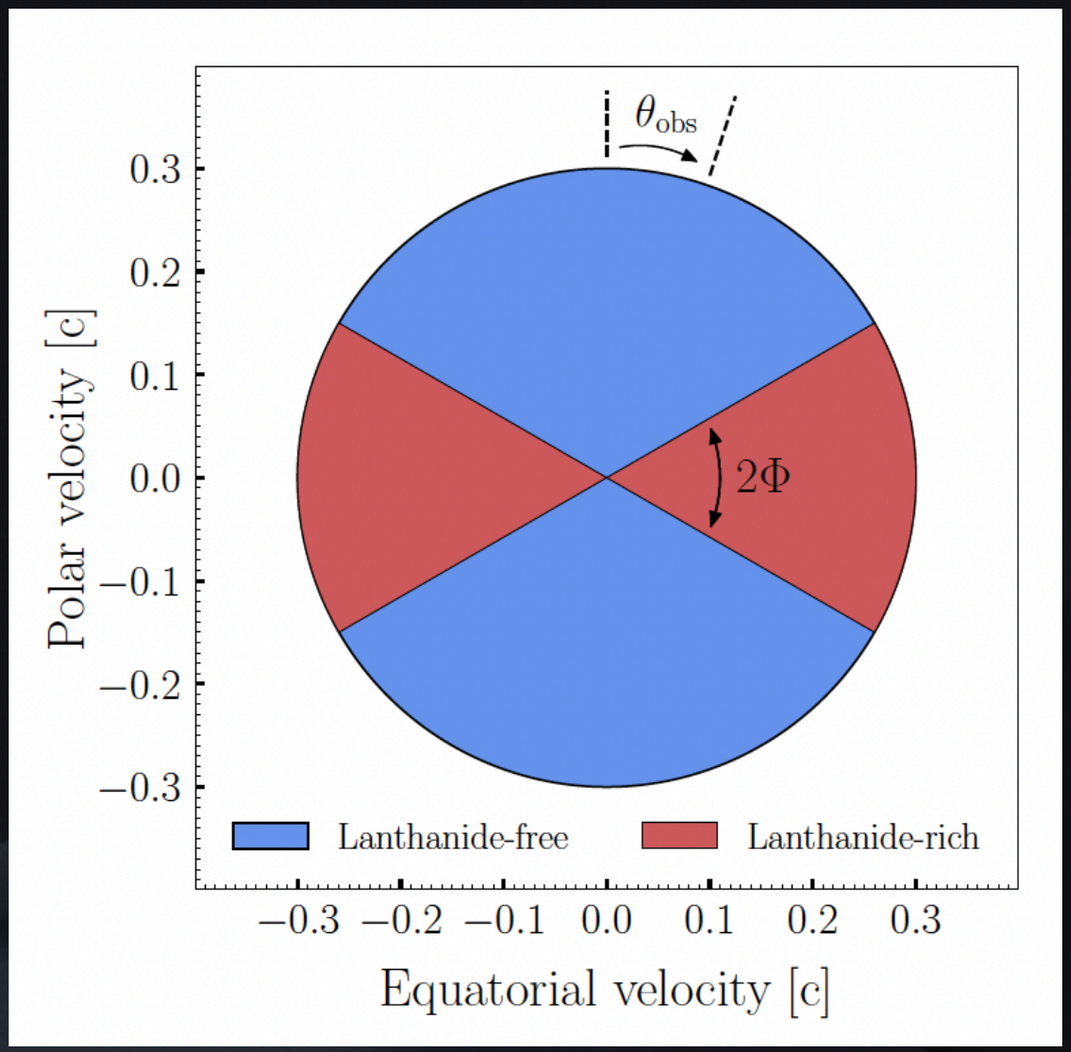

(Bulla 2019)

The faster computation allows to compute 3D, viewing angle dependent models with **interacting** multiple ejecta component...

...and it also allows for a larger exploration of the parameter space

Monte Carlo RT

In both cases MC-RT codes are not fast enough to be used in parameter estimation (e.g. MCMC) studies...

...but we can use them to build a **grid of KN lightcurves** for selected input parameters value...

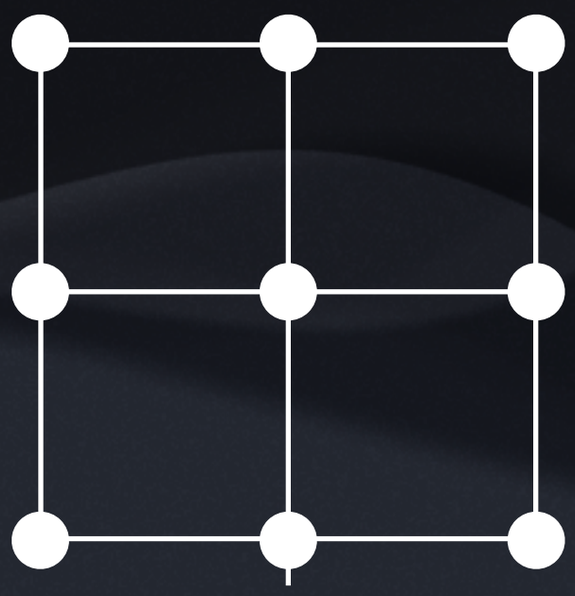

...and make **surrogate kilonova models**, i.e. interpolators/emulators that allows to compute the lightcurve for arbitrary points in the parameter space

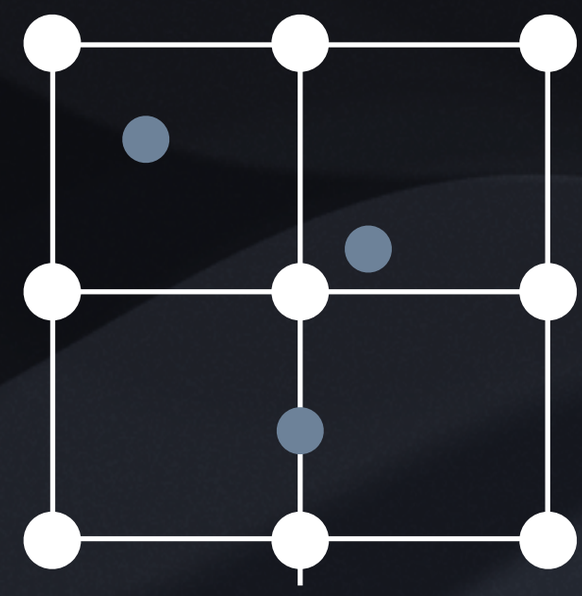

Diffusion in Grey Opacity

Integrating the radiative transfer equation

$$\frac{1}{c}\frac{\partial I_\nu}{\partial t} + \nabla \cdot (\mathbf{n} I_\nu) = j_\nu - \alpha_\nu I_\nu$$

We calculate the 1st and 2nd momenta of RT equation by multiplying by 1 and $\mathbf{n}$ and integrating over $d\Omega$

$$\int (\text{RT eq.}) d\Omega$$

$$\int (\text{RT eq.}) \mathbf{n}\, d\Omega$$

$$\frac{\partial E_\nu}{\partial t} + \nabla \cdot \mathbf{F}_\nu = 4\pi j_\nu - \alpha_\nu c E_\nu$$

$$\frac{1}{c}\frac{\partial \mathbf{F}_\nu}{\partial t} + c\nabla \cdot \hat{P}_\nu = -\alpha_\nu \mathbf{F}_\nu$$

$$E_\nu \equiv \frac{1}{c}\int_{4\pi} I_\nu d\Omega$$ Energy density

$$F_\nu \equiv \int_{4\pi} I_\nu \mathbf{n}\, d\Omega$$ Flux vector

$$\hat{P}_\nu \equiv \frac{1}{c}\int_{4\pi} I_\nu \mathbf{n}\mathbf{n}\, d\Omega$$ Pressure tensor

Diffusion in Grey Opacity

Integrating the radiative transfer equation

$$\frac{\partial E_\nu}{\partial t} + \nabla \cdot \mathbf{F}_\nu = 4\pi j_\nu - \alpha_\nu c E_\nu$$

$$\frac{1}{c}\frac{\partial \mathbf{F}_\nu}{\partial t} + c\nabla \cdot \hat{P}_\nu = -\alpha_\nu \mathbf{F}_\nu$$

We can integrate over frequencies to obtain:

$$\frac{\partial E}{\partial t} + \nabla \cdot \mathbf{F} = \int_0^\infty (4\pi j_\nu - \alpha_\nu c E_\nu) d\nu$$

$$\frac{1}{c}\frac{\partial \mathbf{F}}{\partial t} + c\nabla \cdot \hat{P} = -\int_0^\infty \alpha_\nu \mathbf{F}_\nu d\nu$$

Diffusion in Grey Opacity

Integrating the radiative transfer equation

$$\frac{\partial E_\nu}{\partial t} + \nabla \cdot \mathbf{F}_\nu = 4\pi j_\nu - \alpha_\nu c E_\nu$$

$$\frac{1}{c}\frac{\partial \mathbf{F}_\nu}{\partial t} + c\nabla \cdot \hat{P}_\nu = -\alpha_\nu \mathbf{F}_\nu$$

We apply diffusion approximation

$$\mathbf{F}_\nu = -\frac{4\pi}{3\alpha_\nu}\nabla\frac{j_\nu}{\alpha_\nu} \xrightarrow{\partial_t \mathbf{F} \to 0} \mathbf{F}_\nu = -\frac{c}{3\alpha_\nu}\nabla E_\nu$$

$$\hat{P}_\nu = \frac{1}{3}E_\nu \hat{I}$$

Eddington approx.

Diffusion in Grey Opacity

Integrating the radiative transfer equation

$$\frac{\partial E_\nu}{\partial t} - \nabla \cdot \left(\frac{c}{3\alpha_\nu} \nabla E_\nu \right) = 4\pi j_\nu - \alpha_\nu c E_\nu$$

The idea of Pinto & Eastman 2000 framework, adapted to KNe by Wallaeger+2018 and Ricigliano+2024 (xkn code) is to solve this equation to obtain lightcurve.
In co-moving frame, spherical symmetry and for an homologous expanding ejecta we get

$$\frac{DE}{Dt} - \frac{c}{3r^2}\frac{\partial}{\partial r}\left(\frac{r^2}{\alpha}\frac{\partial E}{\partial r} \right) + \frac{4\dot{R}}{R}E = \dot{E}_{heat}$$

Diffusion in Grey Opacity

Integrating the radiative transfer equation

$$\frac{DE}{Dt} - \frac{c}{3r^2}\frac{\partial}{\partial r}\left(\frac{r^2}{\alpha}\frac{\partial E}{\partial r}\right) + \frac{4\dot{R}}{R}E = \dot{E}_{heat}$$

$$\dot{E}_{heat} \equiv \int_0^\infty (4\pi j_\nu - \alpha_\nu c E_\nu) d\nu = \dot{\epsilon}_r f_{th}\,\rho$$

$$\alpha \equiv \frac{\int_0^\infty \alpha_\nu F_\nu d\nu}{\int_0^\infty F_\nu d\nu}$$

Inverse mean free-path

$$E(r,t) \rightarrow F(r,t) = -\frac{c}{3\alpha}\frac{\partial E}{\partial r} \rightarrow L(t) = 4\pi R^2(t) F(R,t)$$

For given profiles of $\dot{\epsilon}_r(t)$, $f(t)$ analytic solution exists

Diffusion in Grey Opacity

Some Caveats

Contrary to the MC-RT codes, this framework can provide only bolometric luminosities

Moreover, the equation is valid only in the diffusion regime when matter is optically thick

But...

A separate prescription can be (is) implemented for optically thin regions, e.g. in Ricigliano+2024

$$L_{thin}(t) = \sum_{i}^{\text{thin layers}} f_{th,i}(t)\dot{\epsilon}_r(t)dM_i$$

We can assume that the spectral continuum is described by a blackbody at T_{ph}

$$T_{ph} = \max\left[\left(\frac{L_{\text{thick}}}{4\pi R_{ph}^2 \sigma_{SB}}\right)^{1/4}, T_{\text{floor}}\right]$$

Energy Balance equation

Getting back to the start

$$\frac{DE}{Dt} - \frac{c}{3r^2}\frac{\partial}{\partial r}\left(\frac{r^2}{\alpha}\frac{\partial E}{\partial r}\right) + \frac{4\dot{R}}{R}E = \dot{E}_{heat}$$

We integrate over the volume

$$\mathscr{E}_{int} = \int E\, dV \qquad L = \int_S \mathbf{F}\cdot\mathbf{n}\, dS \qquad \dot{Q} = \int \dot{E}_{heat}\, dV$$

$$\frac{d\mathscr{E}_{int}}{dt} = -P\frac{dV}{dt} + \dot{Q}(t) - L(t)$$

Thank you for your attention!

Bibliography

- Abbott et al. 2017, ApJL, 848, L12
- Arnett 1980, ApJ, 237, 541
- Arnett 1982, ApJ, 253, 785
- Ascenzi et al. 2019, MNRAS, 486, 672
- Ascenzi et al. 2021, JPP, 87, 845870102
- Barnes & Kasen 2013, ApJ, 775, 18
- Barnes et al. 2016, ApJ, 829, 110
- Berger et al. 2013, ApJL, 774, L23
- Bulla 2019, MNRAS, 489, 5037
- Bulla 2023, MNRAS, 520, 2558
- Fontes et al. 2017, eprint arXiv:1702.02990
- Grossman et al. 2014, MNRAS, 439, 757
- Levan et al. 2023, Nature Astronomy, 7, 976
- Kasen et al. 2006, ApJ, 651, 366
- Kasen et al. 2017, Nature, 551, 80
- Kasen et al. 2013, ApJ, 774, 25
- Korobkin et al. 2012, MNRAS, 426, 1940
- Kromer & Sim 2009, MNRAS, 398, 1809
- Lodders, 2003, ApJ, 591,1220
- Li & Paczyński 1998, ApJ, 507, L59
- Metzger 2020, LRR, 23, id.1
- Perego et al. 2014, MNRAS, 443,.3134
- Pian et al. 2017, Nature, 551, 67-70
- Pognan et al. 2022, MNRAS, 513, 5174
- Radice et al. 2018, ApJ, 869, 130
- Ricigliano et al. 2024, MNRAS, 529, .647
- Rastinejad et al. 2022, Nature, 612, p.223
- Rosswog et al. 2017, CQG, 34, 104001
- Siegel, 2019, EPJ, 55, 203
- Siegel & Metzger, 2017, PRL, 119, 231102
- Tanaka & Hotokezaka, 2013, ApJ, 775, 113
- Tanaka et al. 2017, PASJ, 69, id.102
- Tanaka et al. 2019, MNRAS, 496, 1369
- Tanvir et al. 2013, Nature, 500, 547
- Villar et al. 2017, ApJL, 851, L21
- Wollaeger et al. 2013, ApJS, 209, 36
- Yang et al. 2024, Nature, 626, 742